Dinoop Lal S. “Photodegradation of polystyrene by nano titanium dioxide and photosensitizers.” Thesis. Research & Postgraduate Department of Chemistry, St. Thomas’ College (Autonomous), Thrissur, University of Calicut, 2020.

Chapter 3

Photodegradation of Polystyrene using Nano TiO_2 and Nano ZnO Catalysts under UV Irradiation - a Comparison

Abstract

Nano TiO_2 has been synthesised by ultrasonication assisted sol-gel technique from Titanium (IV) isopropoxide (TTIP) precursor. ZnO have been synthesised using three methods viz., Sonication assisted precipitation method, hydrothermal method with uncontrolled hydrolysis and hydrothermal method with controlled hydrolysis. TiO_2 and ZnO were characterized using XRD, FTIR spectroscopy, UV-DRS, SEM and EDX. TiO_2 existed as spherical nanoparticles having diameter ≈25 nm. ZnO synthesised through three different techniques resulted in particles of varying size and morphology. XRD analysis revealed that nano TiO_2 existed predominantly in anatase phase with a fewer rutile phase where as ZnO existed in hexagonal wurtzite structure. Photodegradation of PS was studied in the presence of TiO_2 and ZnO under UV radiation. GPC analysis showed a decrease in average molecular weights and increase in chain scission as the time of UV irradiation increased in the PS-composites. FTIR spectra showed that photo-oxidation has taken place in all the composites upon UV irradiation. UV-DRS further supported photodegradation. The mechanical (tensile and flexural) strength of the composites decreased upon UV irradiation. The observed variations in electrical properties (breakdown voltage and dielectric permittivity) of the composites revealed the formation of charged species on UV exposure. Thermal stability of the composites too decreased upon UV irradiation. Based on all the observations it was concluded that PS loaded with TiO_2 or ZnO underwent accelerated UV degradation compared to pristine PS. Photocatalytic efficiency of TiO_2 was found to be superior compared to ZnO for the photodegradation of PS.

3.1 Introduction

The study of photodegradation of solid phase polystyrene (PS) in the presence and absence of nano titanium dioxide (TiO_2) and nano zinc oxide (ZnO) as photocatalysts under UV radiation is reported in this chapter. Even though PS is not a biodegradable polymer and withstands environmental weathering for a long span of time it undergoes photodegradation in the presence of UV radiation from the sunlight[1,2]. Radiations, especially in the UV region are absorbed by polystyrene during photodegradation which causes change in its original properties. Polystyrene undergoes photo-oxidative degradation when exposed to ultraviolet (UV) radiation[3–5]. Photo dissociation (chain scission), formation of carbonyl groups, isolated and conjugated double bonds and slight yellowing occurs due to radical initiated mechanism. Photodegradation cause changes in the original properties of polymer with depleted mechanical properties resulting in weight loss and brittleness[6–11].

Naturally occurring photodegradation of PS is of course a slow process. The rate of photodegradation further depends upon its type (density). High impact polystyrene (HIPS) and general purpose polystyrene (GPPS) takes much longer time to degrade compared to their low density counterparts such as expanded polystyrene (EPS). Difficulty faced by photons to reach the inner layers of high density PS matrix and difficulty to conduct reactive radicals across the tightly packed PS macromolecules are the main reasons responsible for this. This problem could be overcome by the incorporation of photocatalysts into the PS matrix.[12] Loading photocatalysts into PS furnishes more radicals, ions or free electrons in the presence of UV radiation which could further accelerate degradation. Photocatalysts can interact with each other and transfer electrons through the PS matrix where the UV light cannot reach much efficiently. One of the criteria of choosing photocatalysts is that they should have high surface area and very small size[13,14]. Nano particles satisfy these needs. The small size of nano particles resulting in high surface to volume ratio not only enables good and uniform dispersion along the PS matrix but also provides an easy platform for the charge carriers to migrate from the surface of the particles resulting in high photocatalytic activity[15].

Nano metal oxide semiconductor photocatalysts have been celebrated as satisfying photocatalysts for their multi advantages including better efficiency, photostability,

thermal stability, non toxicity, relative cheapness and so on[16–19]. In general semiconductor metal oxides absorb UV or visible radiations of solar spectra resulting to the transfer of electrons from valence to conduction band[20]. The electron hole pair formed further interacts with adsorbed molecules over the surface of these metal oxides resulting in the formation of secondary radicals or ions. These highly reactive species now interacts with the reactant, initiating several radical reactions. Nano TiO_2 and nano ZnO has been the most popular among semiconductor metal oxide especially while dealing with polymer degradation and water purification[21–24]. Herein, a comparative study of nano TiO_2 and nano ZnO on the photodegradation of PS in the presence of UV irradiation is reported.

TiO_2 and ZnO could easily be synthesised in laboratory under normal conditions. The morphology and particle size of these metal oxides could easily be tuned by adjusting the parameters or reaction conditions. In our work, we have used ultra sonication during the formation stage of these metal oxides through which the particle size could be reduced to nano scale. Nano TiO_2 was synthesised by sonication assisted sol-gel route while ZnO was synthesised via sonication assisted hydrothermal and precipitation methods. The synthesised nano particles were used as photocatalysts for the photodegradation of PS. The samples were irradiated using an artificial UV irradiation source and analysed at regular intervals of 200 hour. A comparison of photodegradation of pristine PS with that of PS-TiO_2 and PS-ZnO composites were studied. Variation in mechanical, electrical and thermal properties of the specimens was also studied at regular intervals of UV irradiation.

This chapter is presented in two sections. *Section I* includes the synthesis and characterization of nano TiO_2 and ZnO photocatalysts. *Section II* covers comparative study of photodegradation of PS in the presence and absence of nano TiO_2 and nano ZnO photocatalysts.

Section I

Synthesis and characterisation of nano TiO_2 and ZnO

3.2 Methods

3.2.1 Synthesis of nano TiO_2

Sonication assisted sol-gel method was adopted for the synthesis of nano TiO_2 particles. The precursor used was Titanium (IV) isopropoxide (TTIP). About 0.5 ml of TTIP was added to a mixture of 2 ml ethanol and 2ml deionized water in a boiling tube with constant stirring using a magnetic stirrer. The temperature of the system was set to 50°C. pH 4 was maintained by adding drops of HNO_3. The system was now moved to an ultrasonic probe sonicator (750 W), sonicated for two hours and centrifuged. The settled white precipitate was separated and washed with deionized water several times. Nano particles of TiO_2 collected were dried and calcined at 400°C for 5 hours. The synthesised nano TiO_2 was characterized and used as the photocatalyst for the photodegradation of PS[25–28].

3.2.2 Synthesis of ZnO

Synthesis of ZnO was carried out by three different techniques which resulted in ZnO structures with three different morphologies and particle dimensions. Sonication assisted precipitation method; hydrothermal method with uncontrolled hydrolysis and hydrothermal method with controlled hydrolysis were employed for the synthesis of ZnO as explained below.

Sonication assisted precipitation method:- 0.65 g of $Zn(NO_3)_2.6H_2O$ was dissolved in 25 ml distilled water. The solution was stirred over a magnetic stirrer vigorously to which liquid ammonia was added dropwise. Slow addition of ammonia solution was carried out until the pH of the solution turned out to be 7.5 where precipitation of $Zn(OH)_2$ was assumed to be complete. The system was now subjected to ultrasonic probe sonication for an hour followed by filtration and washing with distilled water. The ZnO powder hence obtained was dried at 80°C for 24 hours and calcinated at 400°C for 5 hours.

Hydrothermal method with uncontrolled hydrolysis:- The same procedure used in precipitation method was repeated in order to obtain turbid solution at pH 7.5. The solution was now transferred into a 50 litre vertical autoclave with distilled water filled up to optimum level. The system was autoclaved for 12 hours at temperature 130 °C. This was now filtered, dried at 80°C for 24 hours and calcinated at 400°C for 5 hours.

Hydrothermal method with controlled hydrolysis:- The same procedure mentioned above was repeated with a change in the autoclave setup. The turbid solution at pH 7.5 was autoclaved in a 25 ml Teflon lined hydrothermal autoclave. The quantity of water in the autoclave was exactly 25 ml. The solution was autoclaved for 12 hours at 130°C followed by filtration, drying and calcination under the same condition as mentioned above to obtain white powder of ZnO[29].

ZnO synthesised through all the three techniques were characterized.

3.3 Results and Discussion

3.3.1 Powder XRD

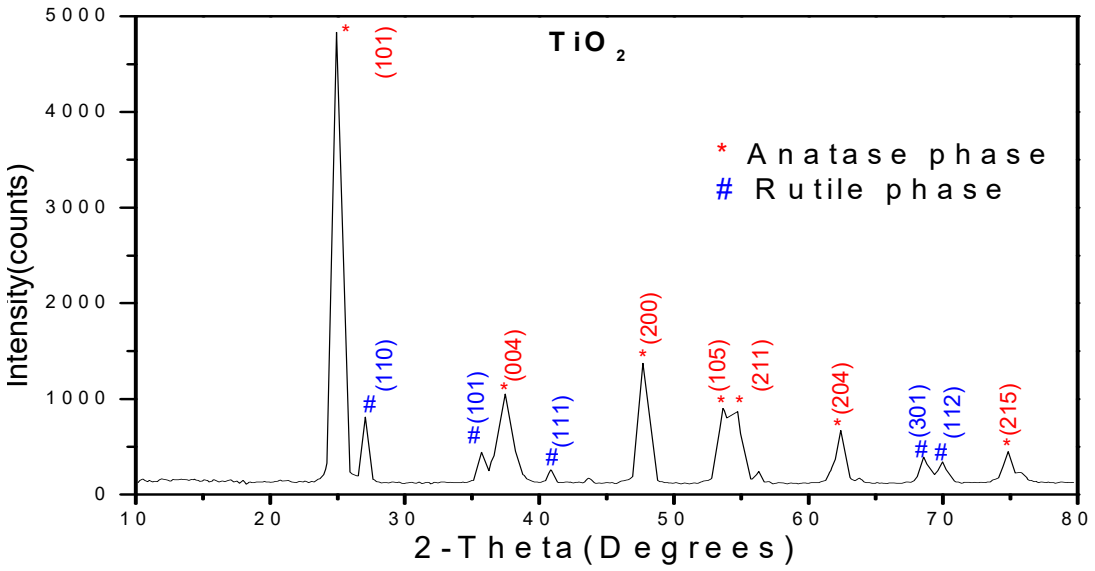

***Figure 3.1.1**. XRD pattern of nano TiO_2 particles*

The powder XRD pattern of TiO_2 synthesised by sol-gel method (Figure.3.1.1) exhibited strong diffraction peaks at 2θ = 24.94° (101), 37.44° (004), 47.70° (200), 53.64° (105), 54.73° (211), 62.40° (204) and 74.80° (215) corresponding to the

anatase phase of TiO_2. The diffraction peaks observed at 2θ = 27.07° (110), 35.71° (101), 40.89° (111), 68.50° (301) and 69.95° (112) indicated the presence of rutile phase of TiO_2 in a lower percentage[30–32]. The percentage of anatase and rutile phases of TiO_2 existing in the composites were determined by Spurr equations (equation 3.1 and 3.2)[33].

Percentage of anatase phase, $A\% = {100}/{\{1 + 1.265\left(\frac{I_R}{I_A}\right)\}}$ (3.1)

Percentage of rutile phase, $R\% = {1}/{\{1 + 0.8\left(\frac{I_A}{I_R}\right)\}}$ (3.2)

Where I_A represents the intensity of anatase (101) peak and I_R represents the rutile (110) peak of TiO_2. The percentage of anatase phase TiO_2 obtained was 91.8 and that of rutile phase was 8.2 %.

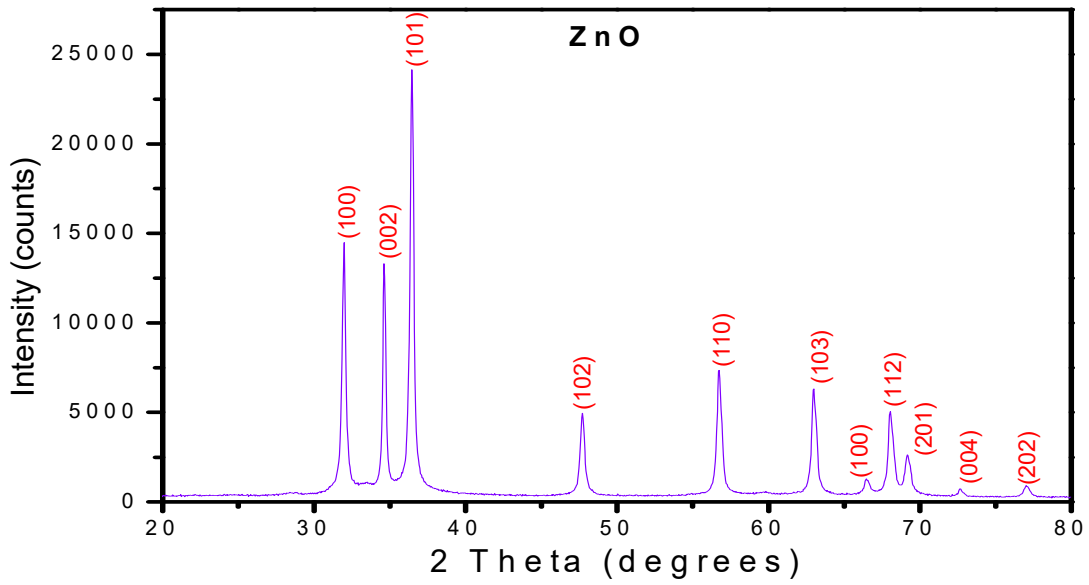

***Figure 3.1.2**. XRD pattern of nano ZnO particles*

ZnO powder synthesised through precipitation as well as hydrothermal methods gave similar XRD patterns (Figure 3.1.2). The XRD pattern of ZnO consisted of peaks at 2θ= 31.97° (100), 34.62° (022), 36.45° (101), 47.71° (102), 56.75° (110), 63.01° (103), 66.48° (100), 68.05° (112), 69.18° (201), 72.70° (004), 77.00° (202). The pattern corresponds to hexagonal wurtzite structure of ZnO. Crystallite sizes of the synthesised TiO_2 and ZnO particles were calculated using the Debye Scherrer's formula (Equation 3.3)[34,35].

$$D = (k.\lambda)/(\beta.\mathrm{Cos}\theta) \quad (3.3)$$

Where

D = Crystallite size (nm)

k = Shape-sensitive coefficient (0.89- For spherical spheres)

λ = Wavelength of the X-ray beam (0.15406 nm for Cu-Kα radiation)

β = Full width at half maximum (FWHM) of the peak under consideration

θ = Diffracting angle

The average crystallite size of TiO_2 particles calculated using Debye Scherrer's formula was 18.9 nm and that of ZnO was 30.7 nm.

Interplanar distance (d spacing) was calculated for each plane of the synthesised TiO_2 and ZnO using Bragg's equation (equation 3.4)

$$\lambda = 2d\sin\theta \quad (3.4)$$

The values of d spacing are as tabulated below (Table 3.1).

Table 3.1. *Interplanar distance d corresponding to each 2θ angles of TiO_2 and ZnO*

TiO_2		**ZnO**	
2 θ°	**d (Å)**	**2 θ°**	**d (Å)**
24.94	3.57	31.97	2.80
27.07	3.29	34.62	2.59
35.71	2.51	36.45	2.46
37.44	2.40	47.71	1.90
40.89	2.21	56.75	1.62
47.70	1.91	63.01	1.47
53.64	1.71	66.48	1.41
54.73	1.68	68.05	1.38
62.40	1.49	69.18	1.36
68.50	1.37	72.70	1.30
69.95	1.34	77.00	1.24
74.80	1.27		

3.3.2 FESEM-EDX

From the FESEM image of the synthesised TiO_2 it could be observed that the synthesised TiO_2 existed as nano particles. The spherical morphology adopted by TiO_2 particles with particle diameter ≈25 nm (as determined through *image j* software) is given in Figure 3.2.1 A. Energy dispersive X-ray (EDX) pattern clearly

confirmed the fact that the synthesised nano TiO_2 particles contained no other impurities (Figure 3.2.1 B). The EDX peaks corresponding to titanium were observed at 4.51 (Kα1), 4.93 (Kβ1) and 0.45 (Lα1) keV and that of oxygen at 0.53 (Kα1) keV. Atomic percentages of titanium and oxygen present in TiO_2 were 19.94 % and 83.06 % respectively according to the EDX pattern.

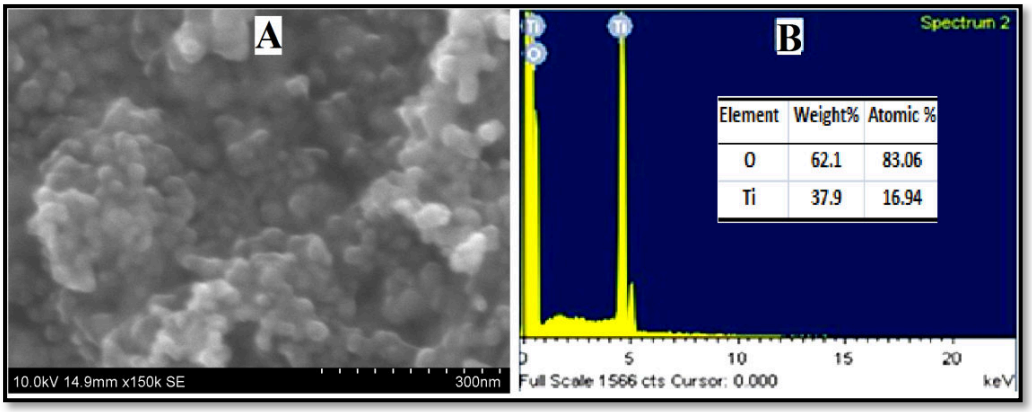

Figure 3.2.1. *FESEM image (A) and EDX pattern (B) of nano TiO_2*

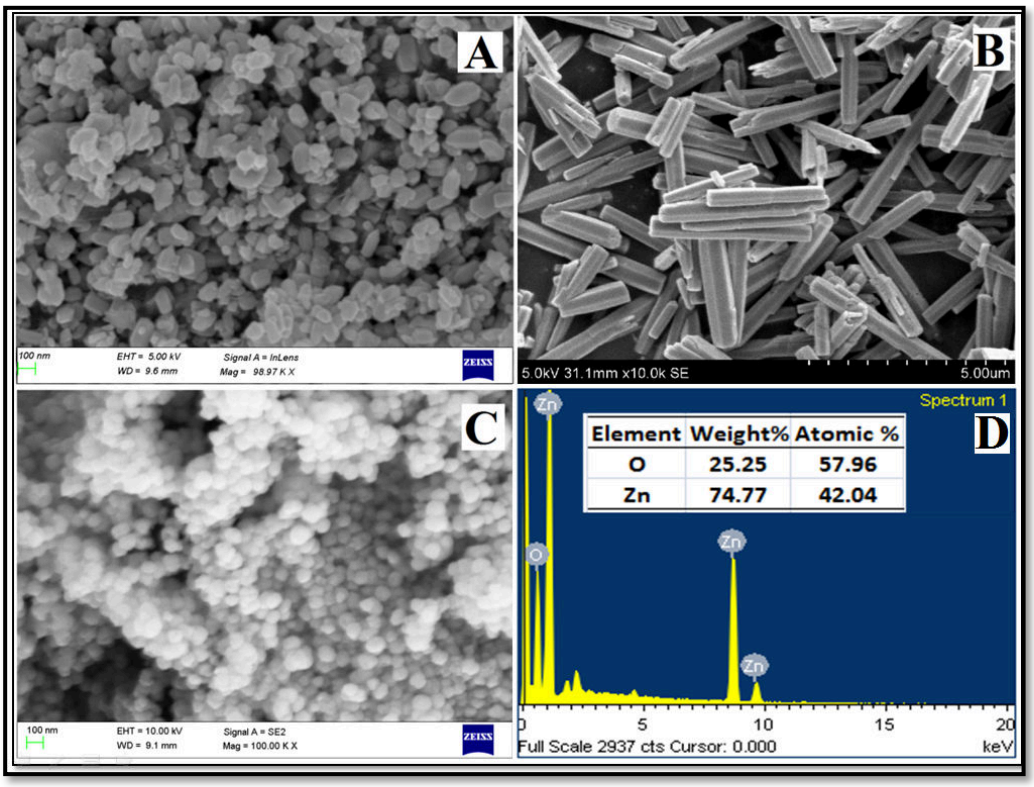

Figure 3.2.2. *FESEM image of ZnO synthesised through: Precipitation method (A) Hydrothermal method (uncontrolled hydrolysis) (B) Hydrothermal method (controlled hydrolysis)(C) and EDX pattern of nano ZnO (D).*

ZnO synthesised through three different synthetic approaches were analysed through FESEM. ZnO synthesised through precipitation method resulted in particles which resembled spheres with irregular edges. As could be seen in Figure 3.2.2 A, the size of the ZnO particles synthesised through this method ranged from 50 to 110 nm with majority of the particles lying in nanometer dimension (<100 nm). Hydrothermal method with excess of water (uncontrolled hydrolysis) adopted for the synthesis of ZnO on the other hand resulted in perfect hexagonal rod shaped structures (Figure 3.2.2 B). Lengths of the ZnO rods were non-uniform and ranges between 0.4 to 5 μm while the thickness of the rods ranges from 250 to 445 nm. ZnO synthesised using hydrothermal method with controlled hydrolysis resulted in nano particles of spherical morphology with diameter ≈70 nm (Figure 3.2.2 C). Controlled hydrolysis was done in a Teflon lined autoclave at a temperature of 120°C. The fact that uncontrolled hydrolysis lead to crystal growth of ZnO whereas controlled hydrolysis resulted in spherical nano structures at 120° C under high pressure were hence clear from the FESEM images. EDX analysis of all synthesised ZnO gave similar pattern which confirmed the presence of zinc and oxygen atoms with no other impurities (figure 3.2.2 D). EDX peaks corresponding to zinc were observed at 1.02 (Lα1, Lβ1 and Lβ3 overlap), 8.62 (overlap of Kα1 and Kα2 overlap) and 9.58 (Kβ1 and Kβ2 overlap) keV. Peak corresponding to oxygen was observed at 0.53 (Kα1) keV.

3.3.3 FTIR Analysis

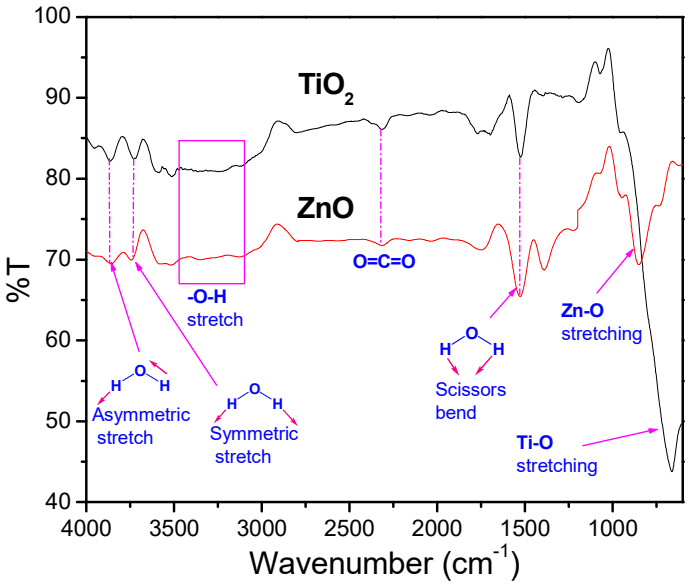

***Figure 3.3**. FTIR spectra of nano TiO_2 and nano ZnO*

FTIR spectra of synthesised nano TiO_2 and nano ZnO is as given in the figure below (Figure 3.3). In addition to Ti-O stretching band (in TiO_2) and Zn-O stretching band (in ZnO), bands corresponding to H_2O, -OH and CO_2 were also observed. The fact that nano ZnO and nano TiO_2 adsorb water, carbon dioxide and hydroxyl ions from the atmosphere was hence clear. The adsorbed H_2O, OH and CO_2 played an important role in the photocatalytic activity of these nano particles under UV radiation (explained section 3.5)

3.3.4 UV- visible Diffused reflectance spectroscopy (UV-DRS)

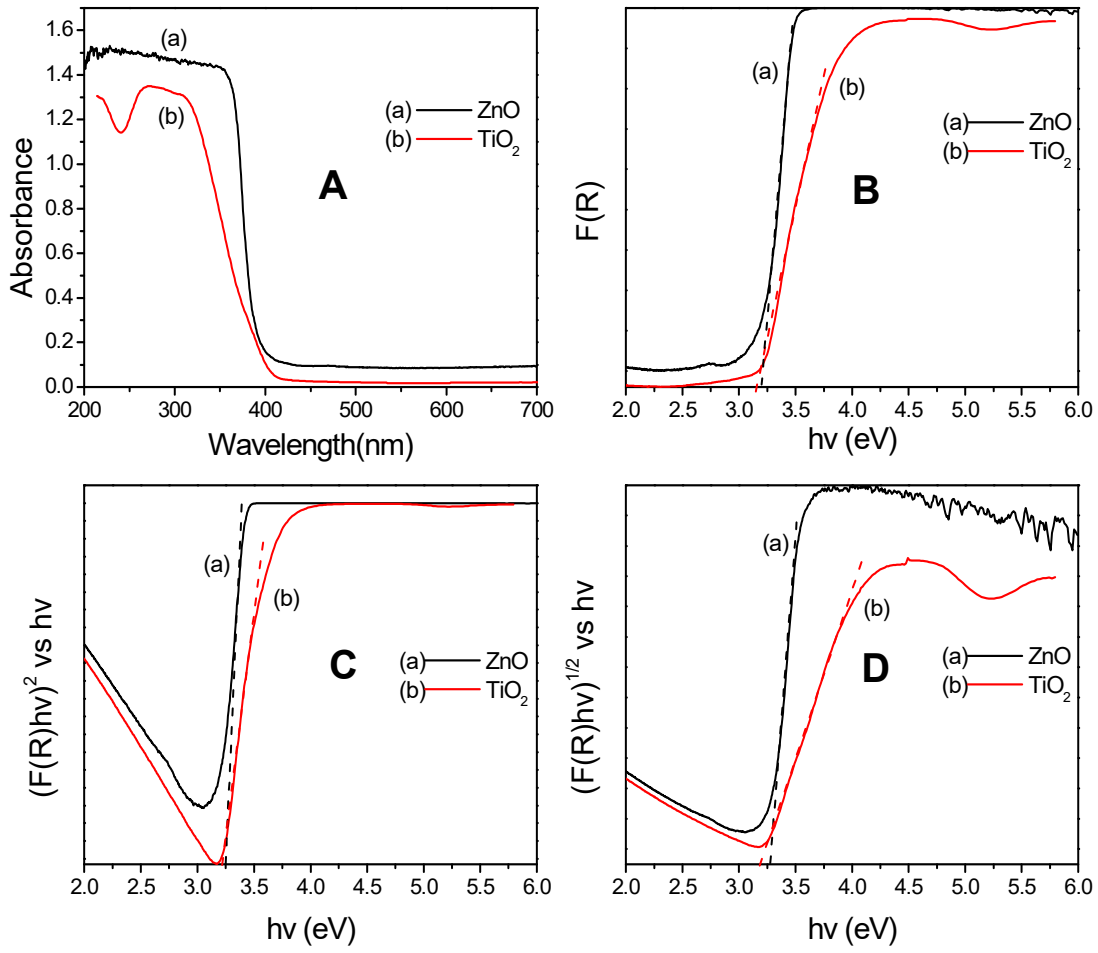

***Figure 3.4**. **A):** Absorption spectra of TiO_2 and ZnO, **B):** Plot of F(R) versus hv **C):** $(F(R)hv)^2$ versus hv representing the direct allowed Eg and **D):** $(F(R)hv)^{1/2}$ versus hv representing the indirect allowed Eg of TiO_2 and ZnO.*

UV-DRS of synthesised TiO_2 as well as ZnO exhibited its characteristic absorption in the UV region (λ<400 nm). No absorption was observed in the visible region (400-800 nm) (Figure 3.4 A). Determination of optical bandgap energies (E_g)

of TiO_2 and ZnO was done by the application of Kubelka-Munk function (K-M or F(R)) in Tauc method[36–38]. Reflectance spectra of the composites obtained through UV-DRS were used for E_g determination. Kubelka-Munk function (F(R)) is given by

$$F(R) = \frac{(1-R)^2}{2R} \quad (3.5)$$

where 'R' is the reflectance.

F(R) was plotted against energy (hυ) in eV and the bandgap energy (E_g) was determined from the plot obtained by extrapolating the linear portion of the curve to the x-axis (Figure 3.4 B). The E_g determined from the plot F(R) v/s hυ was irrespective of transitions (direct/indirect, allowed/forbidden).

In order to determine the E_g of a particular type of transition, F(R) is substituted in Tauc method. Extinction coefficient (α) is related to photon energy and optical bandgap through equation (3.6) according to Tauc method.

$$\alpha = \frac{A(h\upsilon - E_g)^n}{h\upsilon} \quad (3.6)$$

Where *A* is a constant, hυ represents the energy of photons, coefficient (n) is associated with corresponding electronic transition (n=2 for indirect allowed and n=1/2 for direct allowed Eg). F(R) being proportional to α, the following equation (equation 3.7) could be arrived.

$$F(R) = \frac{A(h\upsilon - E_g)^n}{h\upsilon} \quad (3.7)$$

Equation 3.5, known as modified Kubelka-Munk function were used to determine the E_g of TiO_2 of particular transition through the plot of $(F(R)h\upsilon)^n$ v/s hυ. The plot $(F(R)h\upsilon)^2$ versus hυ represents direct allowed transition (Figure 3.4 C) whereas $(F(R)h\upsilon)^{1/2}$ versus hυ represents indirect allowed transition (Figure 3.4D). Modified Kubelka-Munk function also holds further scope for determination of E_gs corresponding to other type transitions just by substituting the exponential factor *n* with corresponding values which is insignificant in this piece of work. The tabulated values of E_gs determined for TiO_2 and ZnO particles using the three methods were as tabulated in the following table (Table 3.2).

***Table 3.2**. Optical bandgap energies (E_gs) of nano TiO_2 and nano ZnO*

Method	Transition Type	Optical Bandgap energy in eV	
		Nano TiO_2	Nano ZnO
F(R) vs hυ	Irrespective of transitions	3.16	3.2
$(F(R)h\upsilon)^2$ vs hυ	Direct allowed	3.22	3.25
$(F(R)h\upsilon)^{1/2}$ vs hυ	Indirect allowed	3.18	3.27

It could be concluded from the comparative values of E_gs that nano TiO_2 has lower E_g compared to nano ZnO. The excitation of electrons from valence band to conduction band in TiO_2 requires lesser energy compared to that of nano ZnO.

Section II

Photodegradation of polystyrene using nano TiO_2 and nano ZnO

PS and PS loaded with TiO_2 or ZnO were prepared using solvent casting method as described in chapter 2. PS, PS-TiO_2 and PS-ZnO composite specimens were also moulded for mechanical and electrical measurements. All the specimens were subjected to UV irradiation. The samples were monitored at regular intervals and the results are as presented below.

3.4 Results and Discussion

3.4.1 Gel permeation chromatography (GPC) analysis

Gel permeation Chromatography analysis of PS, PS-ZnO and PS-TiO_2 was used to determine their average molecular weights ie., weight average molecular weight ($\bar{M}_w$) and number average molecular weight ($\bar{M}_n$). PS, PS-ZnO and PS-TiO_2 composites were subjected to GPC measurements after regular intervals (200 hours) of UV exposure. Average molecular weights of the specimens were measured by GPC and from these data, polydispersity index (PDI), chain scission per macro molecule (S) and number of scission events per gram (N_t) were determined using the equations given below (Equations 3.8, 3.9 and 310).

Average chain scission per polymer macro molecule $S = \left[\frac{(\bar{M}_n)_0}{(\bar{M}_n)_t} - 1\right]$ (3.8)

Number of scission events per gram of polymer $N_t = \left[\frac{1}{(\bar{M}_n)_t} - \frac{1}{(\bar{M}_n)_0}\right]$ (3.9)

Polydispersity index $PDI = \frac{\bar{M}_w}{\bar{M}_n}$ (3.10)

Where $\bar{M}_n$ and $\bar{M}_w$ represents number average and weight average molecular weights of PS respectively. $(\bar{M}_n)_0$ and $(\bar{M}_n)_t$ represents number average molecular weight before and after *t* hours of UV irradiation respectively.

Decrease in average molecular weights were observed in PS as well as PS-composites under study (figure 3.5.1 A & B). Decrease in molecular weights of the polymer specimens could be attributed to the polymer chain scission which in turn was a consequence of polymer degradation on UV exposure.

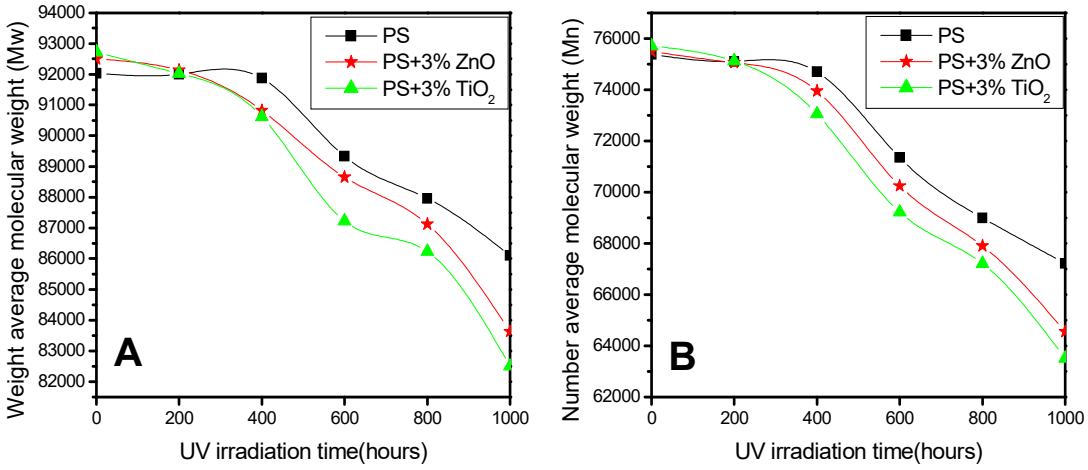

Figure 3.5.1. A): *Weight average ($\bar{M}_w$) and* ***B):*** *number average ($\bar{M}_n$) molecular weights of PS and PS-3% TiO_2 composite under different UV irradiation time*

The increasing value of S and N_t on irradiation (determined using equations 3.8 and 3.9) pointed out the extent to which chain scission had taken place in the polymer specimens on different UV exposure time intervals (Figure 3.5.2 A and B). Decrease in average molecular weights and increase in polymer chain scission were more predominant in PS-TiO_2 composites compared to pristine PS and PS-ZnO composites.

The polydispersity index PDI (calculated from equation 3.10) of the polymer specimens increased with the increase in UV exposure time (Figure 3.5.3). The

increase in the values of PDI reflected the increase in randomness of polymer chain scission. In other words irregular chain breakages lead to the formation of macromolecules of varying molecular masses. It was also clear from GPC data that PS-TiO_2 composites underwent predominant mass loss as well as better chain breakage compared to pristine PS and PS-ZnO. Accounting these facts it could be concluded that TiO_2 acted as a good photocatalyst for the degradation of solid phase PS.

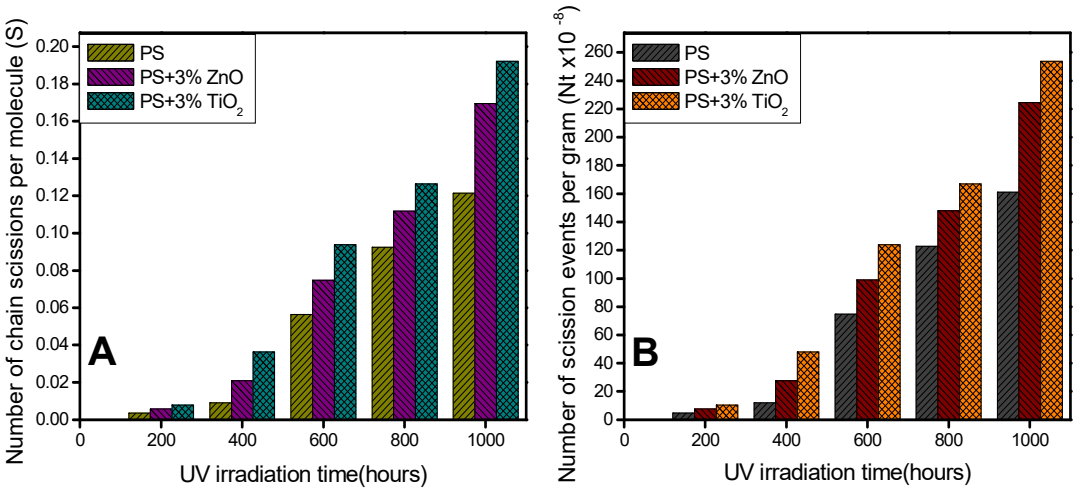

Figure 3.5.2. A): *Number of chain scissions per molecule (S) and* ***B):*** *number of scission events per gram (N_t) of PS and PS-3% TiO_2 composite under different UV irradiation time.*

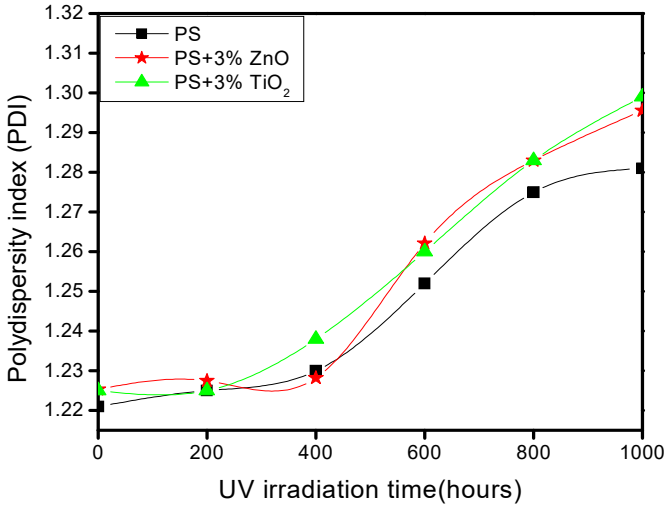

Figure 3.5.3. *Polydispersity index (PDI) of PS and PS-3%TiO_2, PS-3%ZnO composite under different UV irradiation time.*

3.4.2 FTIR Spectroscopy

Changes in chemical structures of the polymer specimens at regular intervals of UV irradiation were investigated through FTIR spectroscopy. Photodegradation of PS and PS composites were further confirmed by FTIR spectroscopy. For the PS and PS composites under study, it was found that the intensities of peaks corresponding to carbonyl (>C=O), hydroxyl (-OH)/ hydroperoxy (-OOH), carbon- carbon double bond (>C=C<), conjugated carbon-carbon double bonds etc stretching vibrations have increased with respect to UV irradiation time. It was also clear from the FTIR spectra that all the functional groups and multiple bonds formed were associated with the PS main chain and not on phenyl rings (Figure 3.6.1, 3.6.2 and 3.6.3).

From the FTIR spectra, it was found that pristine PS and PS composites before and after UV irradiation of regular intervals (200, 400, 600, 800 and 1000 hours) showed characteristic peaks of phenyl ring at around 691 cm^{-1}, 752 cm^{-1}, 905 cm^{-1} and 1027 cm^{-1} with no change in their intensities. These bands attributed to the C-H out of plane bending frequencies of the phenyl ring. The peak at 1448 cm^{-1} corresponding to aromatic carbon-carbon double bond stretch (Ar-C=C- stretch) also showed no change in peak intensity. The above observations show that phenyl rings of PS remain intact after UV irradiation.

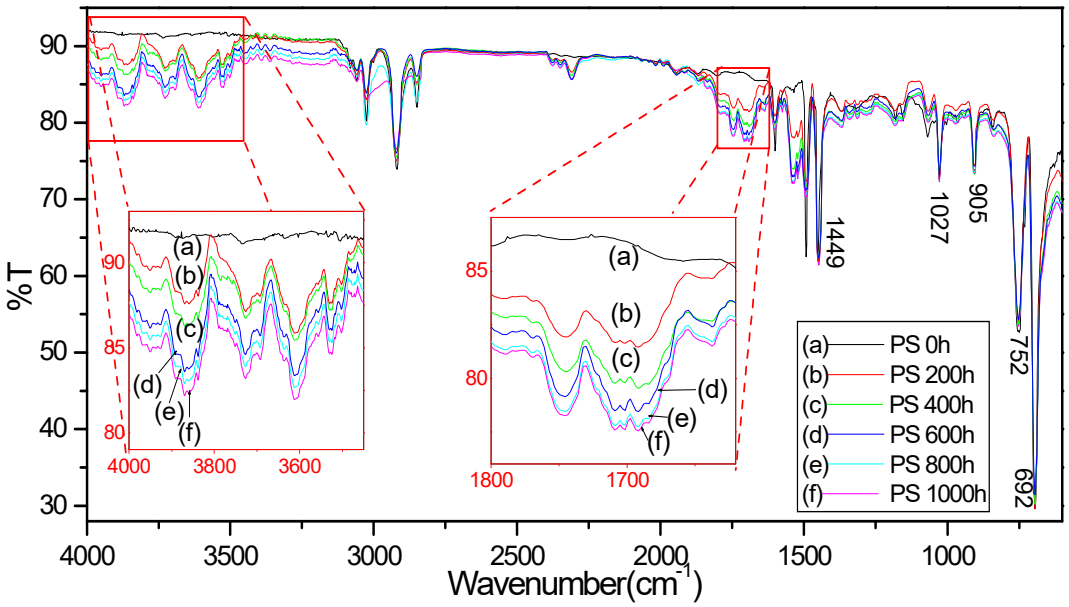

Figure 3.6.1*. FTIR spectra of PS after different UV exposure time intervals ranging from 0 h to 1000 h*

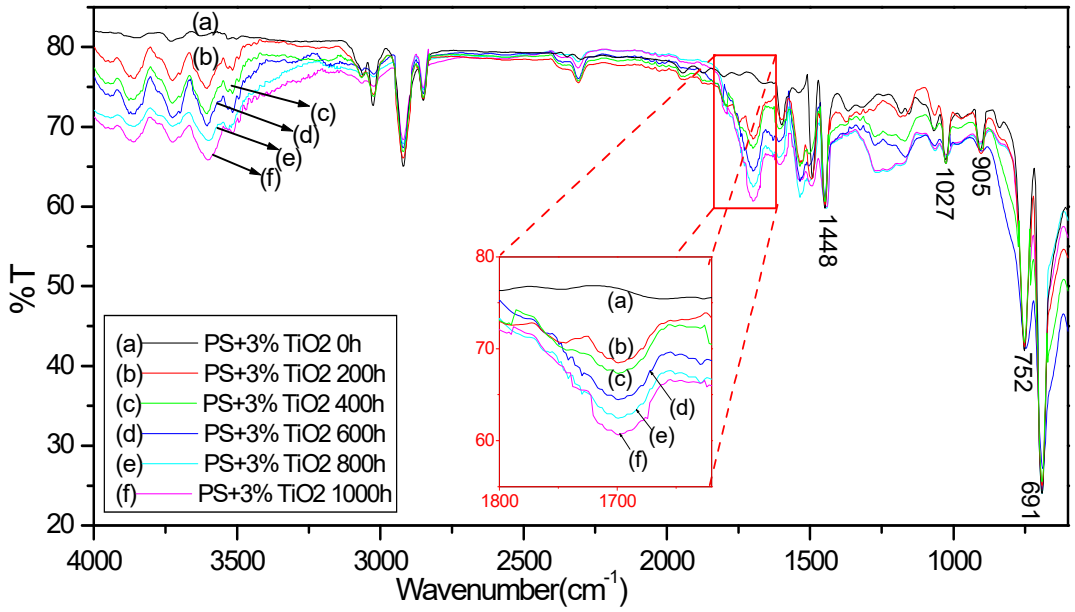

Figure 3.6.2. *FTIR spectra of PS-3%TiO_2 after different UV exposure time intervals ranging from 0 h to 1000 h*

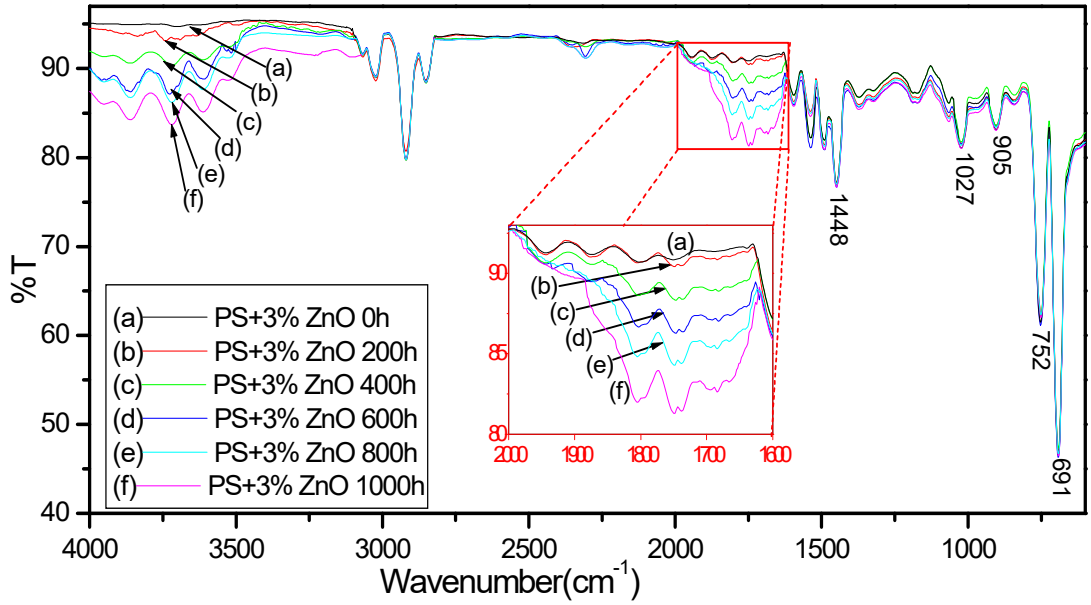

Figure 3.6.3. *FTIR spectra of PS-3%ZnO after different UV exposure time intervals ranging from 0 h to 1000 h*

An increase in the intensity of bands corresponding to carbonyl frequencies ranging between 1750 to 1650 cm^{-1} were observed upon the increase in UV irradiation time. These observations clearly revealed the fact that there was formation and increase in the intensities of carbonyl (>C=O) stretching bands (1740- 1700 cm^{-1}) as well as carbon- carbon double bond (>C=C<) stretching bands (1680-1650 cm^{-1}) upon UV irradiation. The increase in vibrational bands observed at around 1630-1600

cm^{-1} could be assigned to conjugate multiple bond formation upon UV irradiation which was further supported by UV-DRS analysis explained in section 3.4.3 below. The intensity of bands corresponding to hydroxyl and/or hydroperoxy groups (3700-3600 cm^{-1}) also showed an appreciable increase during UV irradiation. Formation of new -OH /-OOH groups upon UV irradiation was established from this observation. The two parameters affecting the increase in the intensities of oxygen containing functional groups and multiple bonds as discussed above were UV irradiation time as well as photocatalyst loading concentrations. FTIR spectra of PS loaded with varying weight percentages of nano TiO_2 (0%, 0.5%, 1%, 2% and 3%) were also analysed. It was concluded that as the percentage of nano TiO_2 loading increased, enhancement in the absorption bands corresponding to -OH, -OOH, >C=O, >C=C<, conjugated carbon-carbon double bonds etc took place for a particular UV irradiation time. Since excess TiO_2 loading (>3% by weight) inversely effected the mechanical properties of PS composite (discussed in section 3.4.6 below), TiO_2 loading was optimized to be 3% by weight, throughout the study. As the entire study is based on comparison between the efficiencies of various photocatalysts for effective photodegradation of PS, The catalytic loading percentages throughout the entire study was focused on 3 weight percentage.

The following conclusions were drawn from the observation made from FTIR spectra. The increase in intensities of >C=O, -OH, -OOH, Ph-C=O etc., functional groups suggested that photo-oxidative mechanism has taken place upon UV irradiation. Increase in the intensities of bands corresponding to >C=C< stretch, conjugated >C=C< , =C-H bend etc suggests that chain and/or bond scission (due to -C–C- or -C-H bond breakage) had taken place (as evident from GPC and supported by UV-DRS). Since there was no change in aromatic >C=C< (stretch) and aromatic -C-H (out of plane bend), it was clear that the phenyl ring remained intact upon UV irradiation. Photo-oxidative degradation of PS-TiO_2 and PS-ZnO composites took place in a more accelerated way compared to pristine PS upon UV irradiation highlighting the efficiency of nano TiO_2 and nano ZnO catalysts. PS-TiO_2 composite (Figure 3.6.2) exhibited predominant photo-oxidative degradation of PS compared to PS-ZnO composite (Figure 3.6.3) confirming the better efficiency of nano TiO_2 compared to nano ZnO.

The observations and conclusions made from FTIR spectra is tabulated below (Table 3.3)

***Table 3.3**. Important observations made from FTIR spectra of PS and PS-composites.*

IR vibration peaks	Assigned functional groups	Change in intensity up on UV irradiation
3700-3600 cm^{-1}	Free –OH/-OOH	Intensity increased
1740-1700 cm^{-1}	>C=O stretch	Intensity increased
1680-1650 cm^{-1}	>C=C< stretch	Intensity increased
1630-1600 cm^{-1}	Conjugated >C=C< stretch	Intensity increased
1452 cm^{-1}, 1600 cm^{-1}	Aromatic >C=C< stretch	No change
1027, 905, 752, 691 cm^{-1}	Ar C-H (Out of plane bend)	No change
830 cm^{-1}	Conjugated >C=C< bend	Intensity increased
650 cm^{-1}	=C-H bend	Intensity increased

3.4.3 UV-visible Diffused Reflectance Spectroscopy (UV-DRS)

UV-visible diffused reflectance spectra (UV-DRS) of pristine PS, PS-TiO_2 and PS-ZnO showed notable changes in their characteristic absorption bands upon UV exposure (Figure 3.7.1 A, B & C). An appreciable decrease in the absorption peaks of the polymer specimens under study were observed in the UV region (between 230-400 nm) with respect to the increase in UV irradiation time. This observable hypochromic effect reflected degradation of polymer chain. As evident from FTIR spectra explained above the increase in >C=O ($n \rightarrow \pi^*$) absorption bands with UV exposure time could not be identified over this area (230-290 nm) due to their low intensity. Depletion of polymer chain lead to a decrease in the absorption bands that dominated the formation of >C=O groups which should otherwise have caused an increase in intensity (due to $n \rightarrow \pi^*$ transition) over this area (230-290 nm). The region of UV spectra with wavelength below 230 nm showed an increase in absorption bands with respect to UV irradiation time. This hyperchromic effect could be due to the

increase in the absorption bands of -OH (n→π*), >C=O (π →π*) and >C=C< (π →π*) functional groups upon irradiation. Another striking trend observable from the UV-vis spectra was an increased bathochromic shift (red shift) and slight increase in absorption intensity in the visible region with respect to the irradiation time for all specimens. Formation and increase in conjugated double bonds between carbon atoms was evident from this observation. The observable trends as mentioned above of UV DRS were predominant in PS-TiO_2 composites. UV DRS hence supports the fact that TiO_2 is a better catalyst compared to ZnO for the photodegradation of PS under UV radiation.

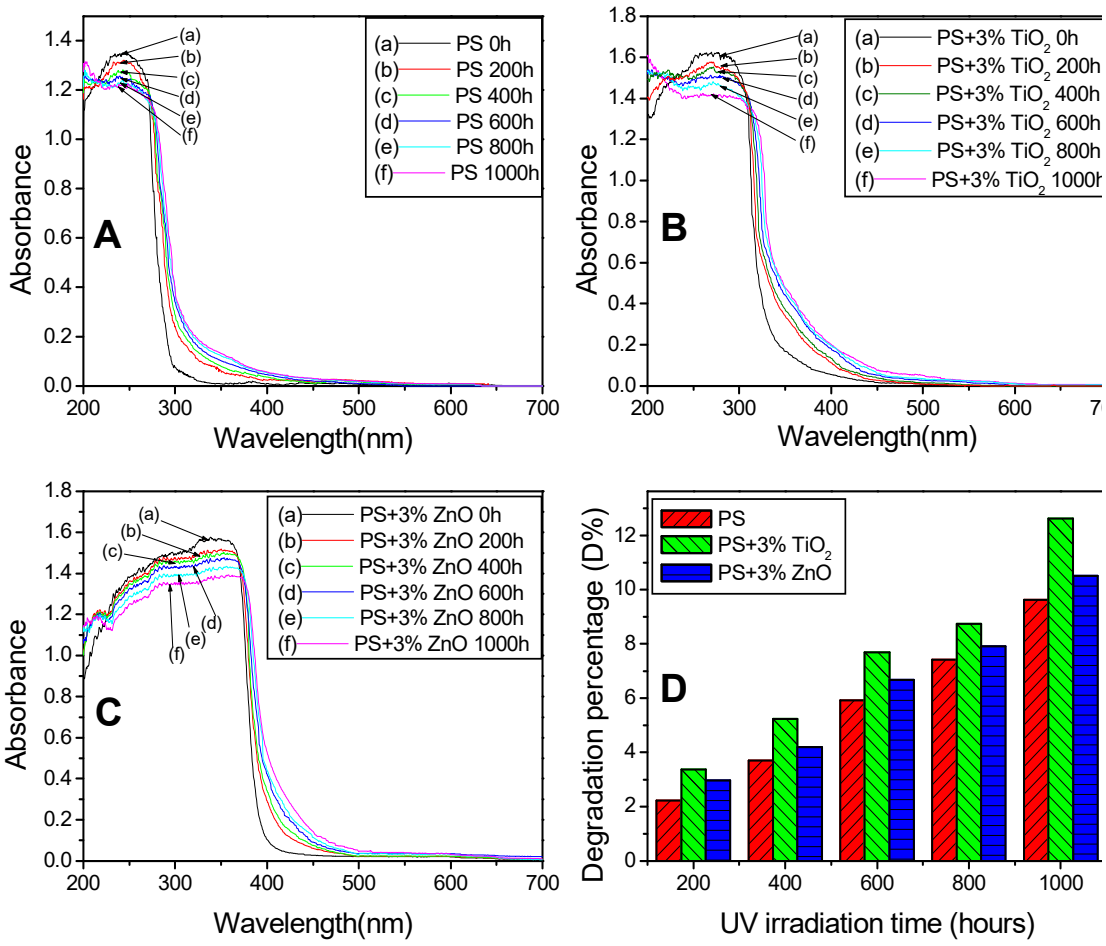

Figure 3.7.1*. UV-DRS of PS (A), PS-3%TiO_2 (B) and PS-3%ZnO (C) at regular UV irradiation intervals and their degradation percentages (D%).*

The percentages of photodegradation (D%) at each time interval of UV irradiation were calculated using equation 3.11 from UV-visible spectra.

$$D\% = \left(\frac{A_0 - A}{A_0}\right) X100 \quad (3.11)$$

Where A_0 and A represents the absorption maxima of the polymer specimens before and after UV irradiation respectively.

D% was found to be higher for PS-TiO_2 composites compared to PS-ZnO and pristine PS (Figure 3.7.1 D). The D% of PS, PS+3%ZnO, PS+3%TiO_2 after 1000 hours UV exposure was 9.63, 10.56 and 12.62 % respectively. In other words the degradation efficiency of photodegradation of PS has increased upon loading it with ZnO or TiO_2.

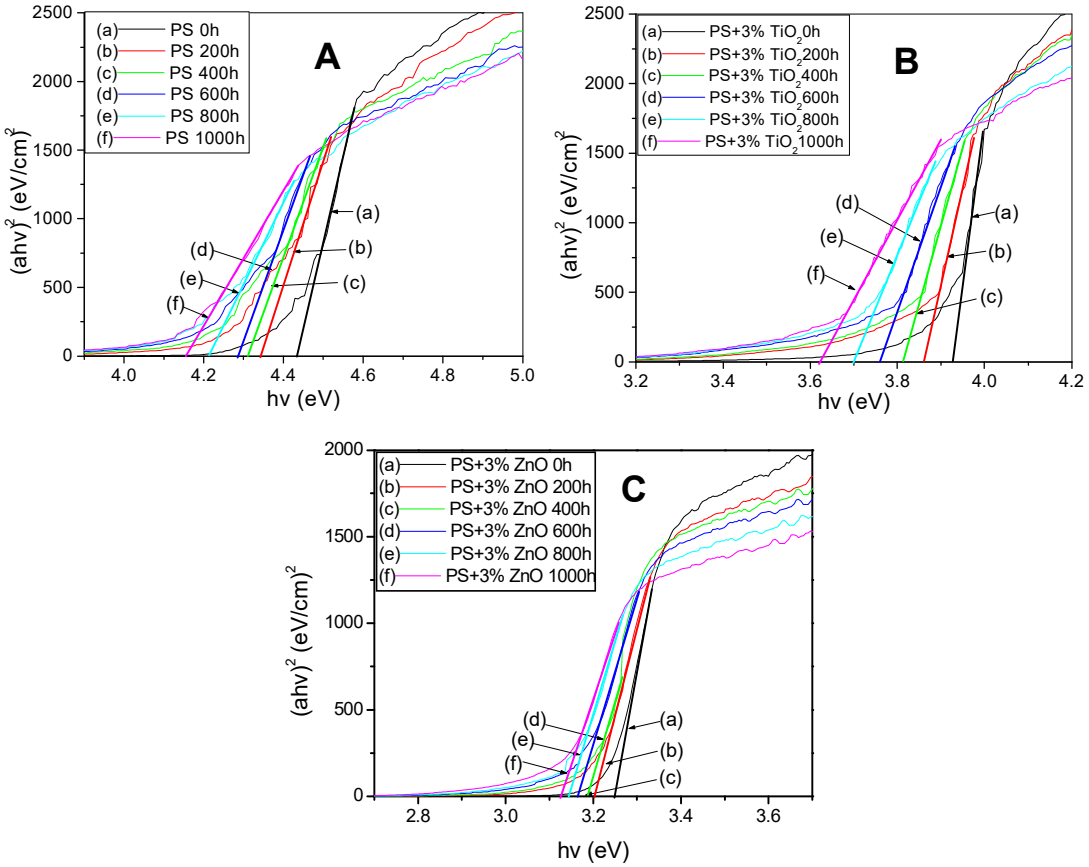

Figure 3.7.2. *Optical bandgap energy determination from the plot of $(\alpha h\upsilon)^2$ v/s $h\upsilon$ for PS (A), PS-3%(TiO_2) (B) and PS-3%ZnO) (C) subjected to different UV exposure time intervals ranging from 0 h to 1000 h*

Optical bandgap energy (E_g) of PS, PS-TiO_2 and PS-ZnO films before and after UV irradiations of different intervals were determined using Tauc relation (Equation 3.12)[39–43].

$$\alpha h\upsilon = A(h\upsilon - E_g)^n \quad (3.12)$$

Where α is the absorption coefficient, hυ is the energy of photon in eV (h= Plank's constant and υ = frequency of radiation), A is a constant (different for different transitions), E_g is the bandgap energy and the index n is assumed to have different values corresponding to different electronic transitions (n= ½ for direct allowed transition and n=2 for indirect allowed transition)

A plot of $(\alpha h\upsilon)^2$ versus hυ gave the direct allowed bandgap energy (E_g) of PS as well as PS composites, on extrapolating the linear portion of the curve to the X axis (where α=0) (Figure 3.7.2). The E_gs for PS as well as PS-composites showed a decrease in value upon increase in the time of UV irradiation. E_g of PS, PS-3% TiO_2 and PS-3% ZnO were determined to be 4.43, 3.93 and 4.04 eV respectively. The decrease in E_g of PS-TiO_2 and PS-ZnO composites in comparison with pristine PS was hence clear.

3.4.4 Scanning electron microscopy (SEM)

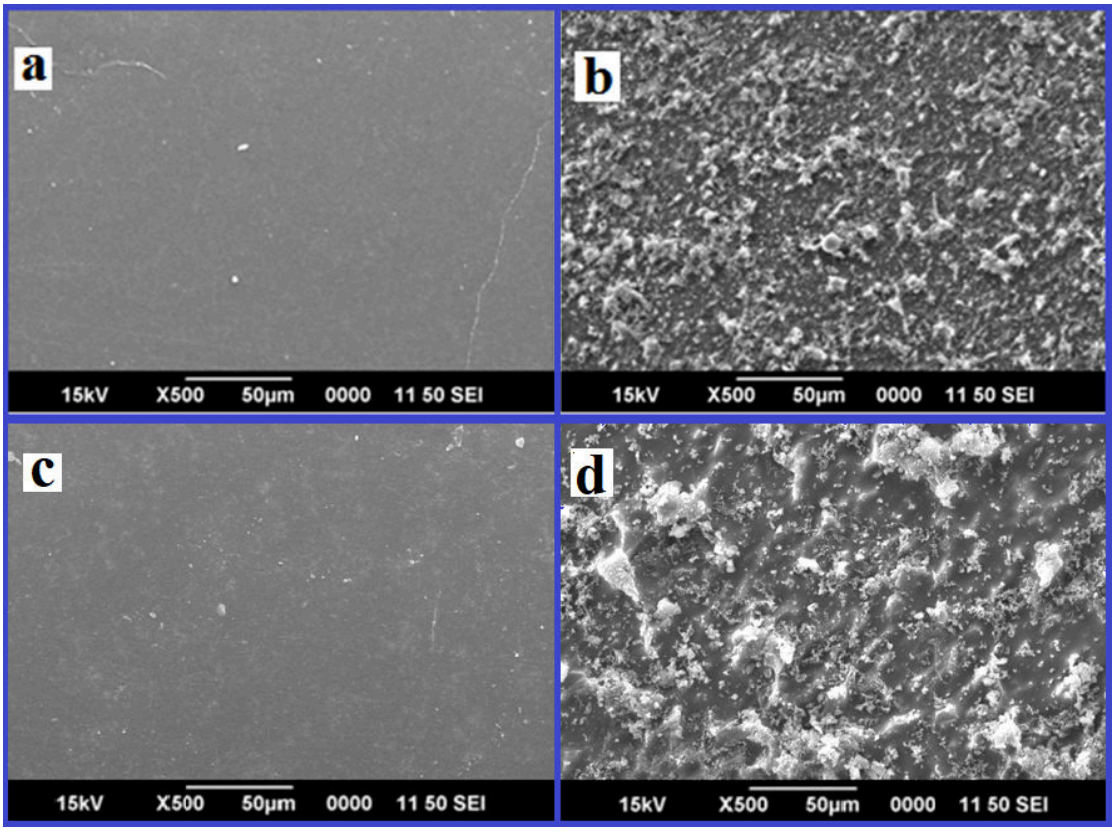

***Figure 3.8**. SEM image of PS-3%TiO_2 and PS-3%ZnO respectively before (a & c) and after (b & d) UV irradiation of 1000 h*

The change in surface morphology of the UV irradiated PS composites as a consequence of photodegradation was observable from their SEM images. Figure 3.8 a & c represents the SEM images of PS-3%TiO_2 and PS-3%ZnO respectively before UV irradiation and figure 3.8 b & d show these composites after 1000 hours of UV exposure. The increase in the surface roughness upon UV irradiation as a result of photodegradation could be clearly identified from figure 3.8 b &d when compared with figure 3.8 a and c.

3.4.5 Thermogravimetric Analysis (TGA)

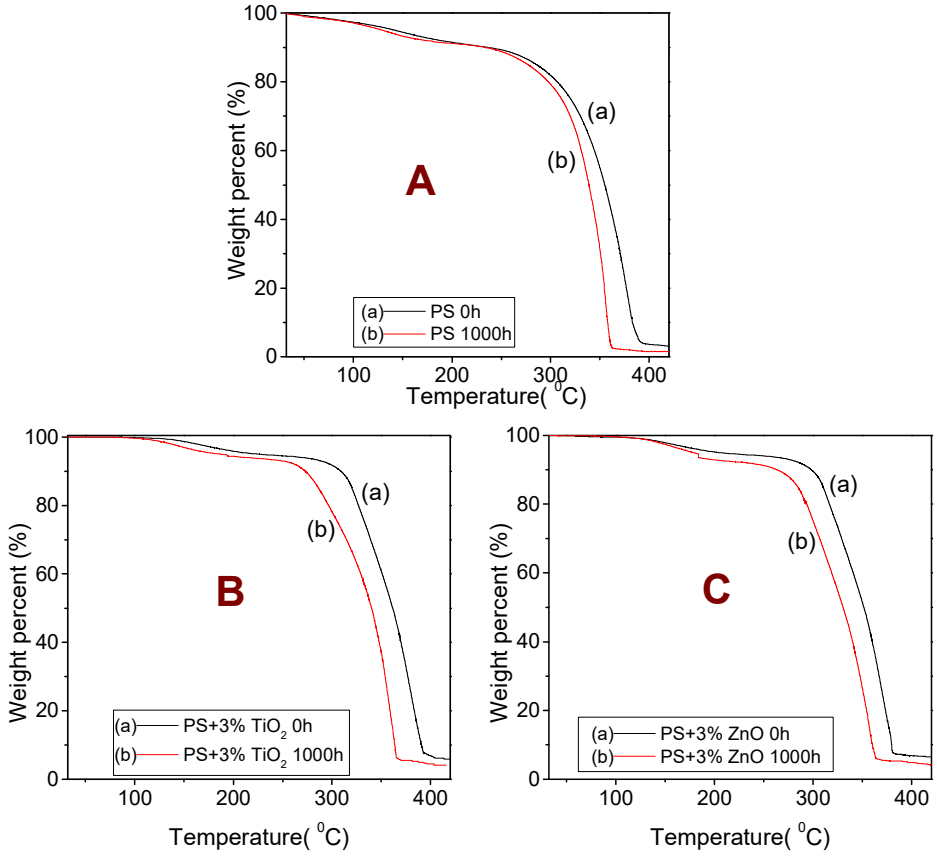

Figure 3.9. *TGA thermogram of PS, PS-3%TiO_2, PS-3%ZnO before and after UV irradiation of 1000 h*

TG analysis was conducted in an inert atmosphere by circulating nitrogen gas continuously through the sample holding crucible. From the TGA thermogram it was observed that the decomposition temperature of PS-ZnO and PS-TiO_2 composites were higher compared to that of pristine PS (Figure 3.9).

The first stage of weight loss for PS and PS-composites observed at a temperature around 118°C may attribute to the desorption of water molecules. The decomposition temperature of PS observed at 252-394°C increased for the PS composites (269-380°C for PS+3% ZnO composite and 272-407°C for PS+3% TiO_2 composite). The increase in decomposition temperature of PS composites highlighted the fact that the thermal stability of PS has increased upon nano ZnO and nano TiO_2 loading. It was also observed that decomposition temperature of UV irradiated PS and PS composites decreased appreciably compared to their unirradiated counterparts. UV irradiation of PS and PS-composites lead to the breakage or weakening of polymer chains, resulting to a decrease of decomposition temperature. PS loaded with ZnO and TiO_2 catalysts exhibited higher thermal decomposition compared to pristine PS under UV irradiation. Higher thermal decomposition rate under UV irradiation was observed in PS-TiO_2 composite highlighting the fact that nano TiO_2 has caused better photodegradation over the PS matrix compared to nano ZnO.

3.4.6 Mechanical Properties of PS, PS-TiO_2 and PS-ZnO composites

Flexural and tensile properties of PS and PS composites were determined using a universal testing machine (UTM) before and after UV irradiation of certain intervals.

The stress-strain graph (Figure 3.10.1) of PS, PS-TiO_2 and PS-ZnO looked similar with no visible area under the curve. This observation could lead us to the conclusion that PS and PS composites under study were strong but not very tough. If the polymer specimens were tough and elastic, a smooth curve of higher surface area would have been observed instead of steep slope with sudden break. PS composites of nano TiO_2 and ZnO showed enhanced tensile property compared to pristine PS. The value of tensile strength of pristine PS observed at 52.92 MPa was found to have increased with the increasing percentage of nano TiO_2 loaded up to 3% by weight (tensile strength=53.23 MPa). At 5% by weight of nano TiO_2 loading the value of tensile strength showed a decrease in value (52.95 MPa) instead of increasing (Figure 3.10.2 A). Due to this reason, 3% nano TiO_2 loading in PS was considered to be the optimum catalytic concentration and throughout the study 3% catalyst loading was considered for various other investigations regarding photodegradation studies. A comparison of tensile properties of PS, PS-3% ZnO and PS-3%TiO_2 was made and it was found that the value of tensile strength found to be 52.92 MPa in PS increased up to 53.12 MPa

in PS-3% ZnO and 53.23 MPa in PS-3%TiO_2 composite. The enhancement in the tensile property suggested strong binding between nano TiO_2 /nano ZnO particles and PS chains preventing an easy break. PS loaded with nano TiO_2 or nano ZnO could enhance the strength of PS but could not enhance its toughness as evident from the steep stress-strain plot with almost no area under the curve. The superior mechanical properties demonstrated by PS nano composites over pristine PS promises the scope of their wide applications in various sectors where strength of the polymer material remains primary concern. The tensile strengths of PS, PS-TiO_2 and PS-ZnO decreased as the time of UV irradiation increased (Figure 3.10.3 A). The decrease in tensile strength attributed to the weakening or cleavage of bonds in polymer chain as a consequence of photodegradation upon UV light exposure. Nano TiO_2 and nano ZnO loaded PS composites underwent better decrease in tensile values under UV irradiation. Maximum decrease in the tensile strength upon UV irradiation was observed in PS-TiO_2 composites compared to pristine PS and PS-ZnO composites under study.

Flexural properties of PS and PS composites displayed similar trend as that of their tensile properties. Here too an enhancement in the flexural strength of PS was observed as the percentage of nano TiO_2 loading increased (Figure 3.10.2 B). The flexural strength observed for PS at 82.98 MPa increased drastically to 86.96 MPa in PS-3% ZnO and to 87.24 MPa in PS-3%TiO_2 (Figure 3.10.3 B). UV exposure resulted in a decrease in the values of flexural strengths as observed in the case of tensile strengths of the specimens. Maximum decrease in flexural strength upon UV irradiation was observed in PS-TiO_2 composites compared to other specimens under study, as observed in the case of tensile strength.

Depletion of mechanical property as a consequence of chain degradation was clearly understood from the above observation. The fact that nano TiO_2 and nano ZnO acted as good photocatalysts leading to photodegradation of PS was further supported by the study of mechanical properties of the composites. Nano TiO_2 proved to be more efficient compared to nano ZnO for the degradation of PS photochemically. Deterioration of mechanical properties of PS composites upon UV irradiation leads to their easy destructions in an accelerated way.

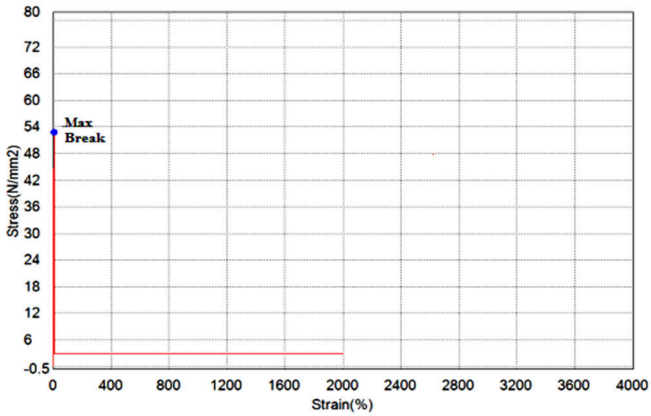

Figure 3.10.1. *Stress-strain plot of pristine PS*

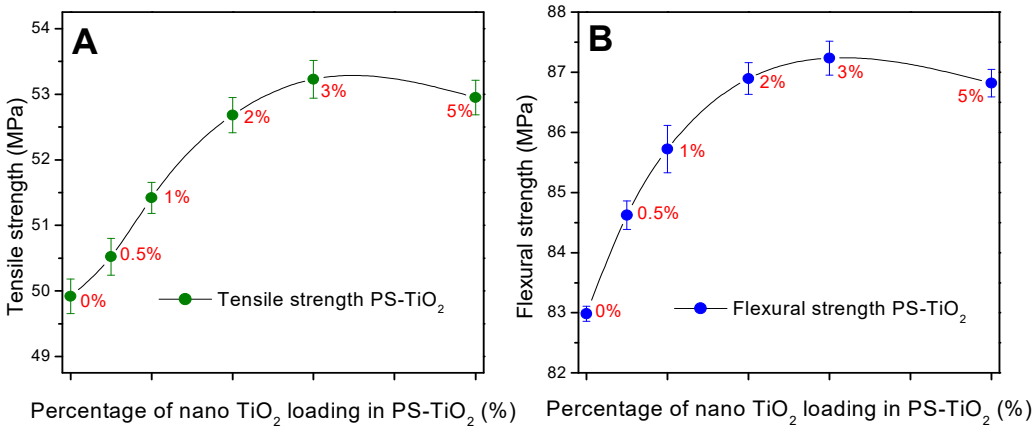

Figure 3.10.2. *Tensile (A) and flexural (B) strengths of PS with different weight percentages of TiO_2*

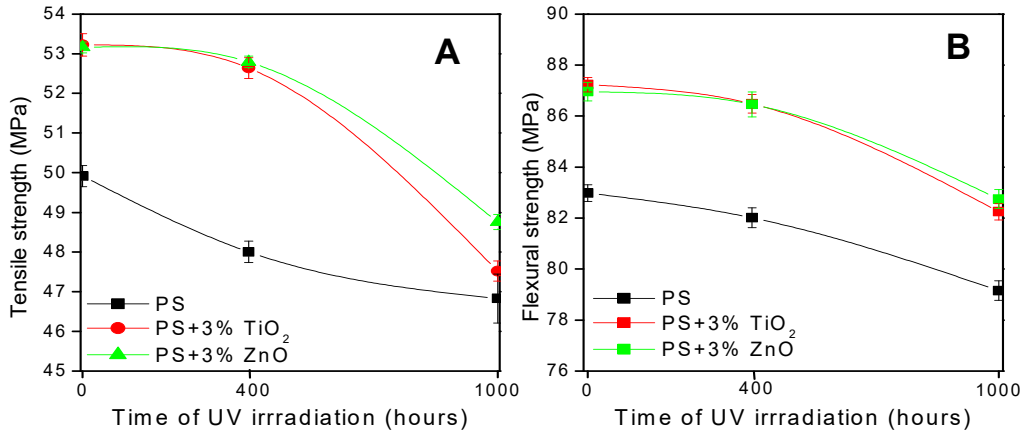

Figure 3.10.3. *Tensile (A) and flexural (B) strengths of PS, PS-TiO_2 and PS-ZnO composites exposed to UV radiation for 0, 400 and 1000 h*

3.4.7 Electrical Properties of PS, PS-TiO_2 and PS-ZnO composites

Dielectric breakdown or Breakdown voltage (BDV) and dielectric permittivity of the polymer specimens were measured. BDV of the polymer samples measured in

alternating current of frequency 50Hz is as illustrated in Figure 3.11.1. The BDV of PS before UV irradiation was determined to be 25.17 kV/mm. The BDV of PS-TiO_2 and PS-ZnO composites showed an increased value having 30.03 and 29.11 kV/mm respectively. The increased value of BDV of PS-TiO_2 and PS-ZnO composites indicated the existence of electron trapping and scattering interfaces between the polystyrene matrix and nano TiO_2/ZnO particles[44]. The dielectric breakdown of all the specimens decreased upon UV irradiation. The decrease in BDV with respect to UV irradiation time could be attributed to the formation of charge centers due to photodegradation. As evident from FTIR spectra, UV- DRS and GPC, the PS chain underwent chain scissions and photo-oxidation upon UV irradiation which had taken place through various ions/radical intermediates leading to the accumulation of charge centers over the polymer matrix. The charge centers formed along the polymer chain as a consequence of photodegradation lead to the flow of electric current much easier through the polymer matrix resulting in the breakdown of the specimens at comparatively lower voltage applied (lower BDV)[44]. Decrease in the BDV upon UV irradiation was predominant in PS-TiO_2 composite compared to PS and PS-ZnO composites.

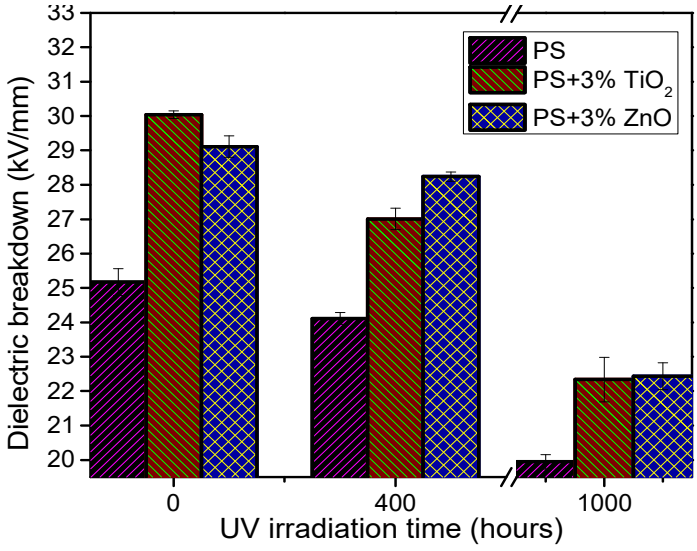

Figure 3.11.1. *Dielectric breakdown (breakdown voltage) of PS, PS-3%TiO_2 and PS-3%ZnO at varying UV irradiation time*

Dielectric permittivity (ε_r) of the polymer specimens were calculated from their determined capacitance value using equation 3.13[45,46].

$$C = \varepsilon_r \, \varepsilon_0 \left({}^{A}/_{t}\right) \qquad (3.13)$$

Where, C is the capacitance; ε_r is the dielectric permittivity; ε_o is the dielectric permittivity of free space (8.854×10^{-12} F/m); A is the area and t is the thickness of the polymer specimens.

The composites (PS-TiO_2 and PS-ZnO) exhibited better dielectric permittivity (ε_r) compared to that of pristine PS (Figure 3.11.2). The ε_r of PS as well as PS composites increased upon UV irradiation. The formation of charge centers/dipoles as a result of photodegradation of PS resulted to an increase in ε_r which could most predominantly be seen in PS-TiO_2 composite compared to the other specimens.

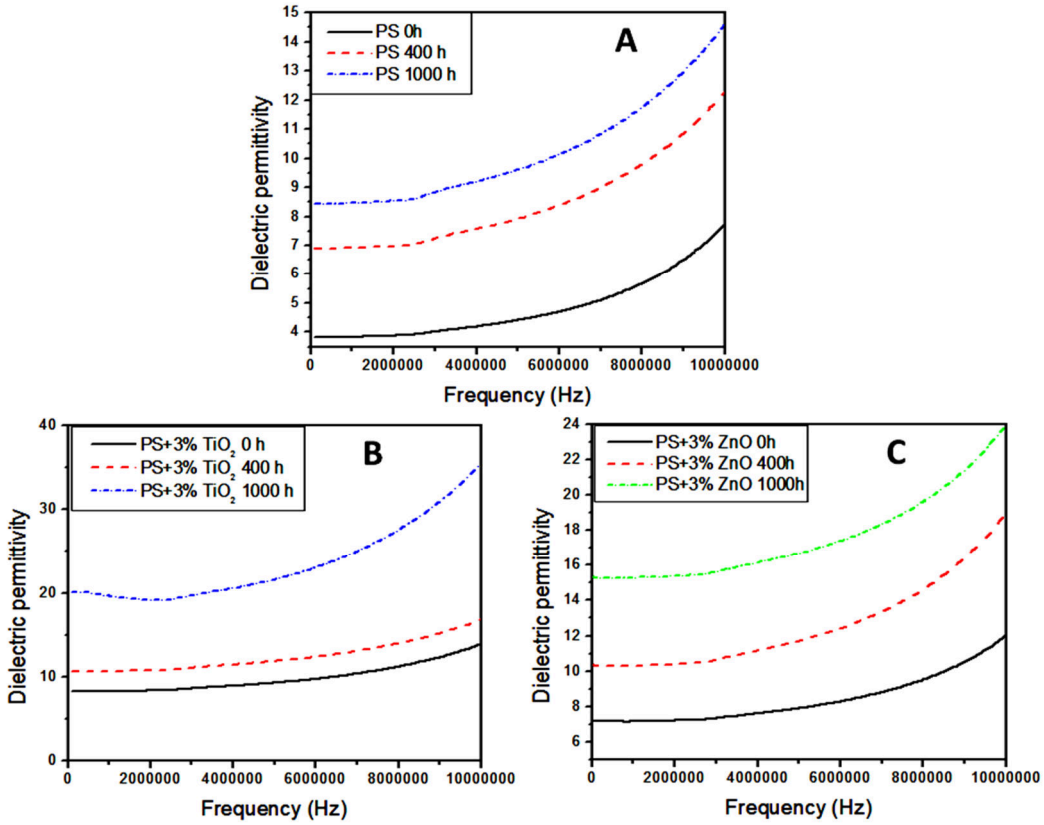

***Figure 3.11.2**. Dielectric permittivity of PS, PS-3%TiO_2 and PS-3%ZnO at UV irradiation intervals of 0 h,400 h and 1000 h.*

3.4.8 Weight loss measurement

Weight loss of pristine PS as well as PS-composites was measured regularly after 200 hours of UV exposure time under same conditions. A considerable weight loss was observed in the samples with increase in the time of exposure. It was also found that the weight loss of TiO_2 loaded PS was found to be higher compared to that of PS-ZnO and pristine PS as shown in Figure 3.12. The observed weight loss may be due to

the escape of volatile species during the photodegradation process. Diffusion of H•, O_2•, OH• and OH_2• radical species created upon UV light exposure of the composites (as discussed in the forthcoming section 3.5) could diffuse through the polymer matrix leading to the formation of carbon centered radicals[47]. Successive radical interactions result in polymer chain cleavage with oxygen getting incorporated to the carbon center causing evolution of gases like CO_2, CO etc[48]. The interaction of H• and O_2• could also lead to the formation and evolution of H_2O molecules.

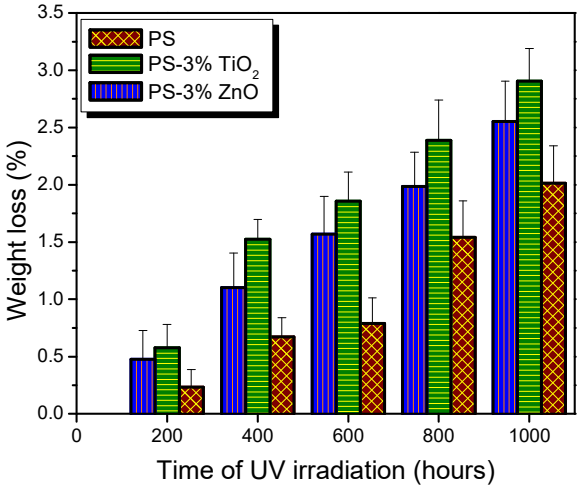

Figure 3.12. *Weight loss percentages of PS, PS-TiO_2 and PS-ZnO Composites at regular intervals of UV irradiation*

3.4.9 Visual observations

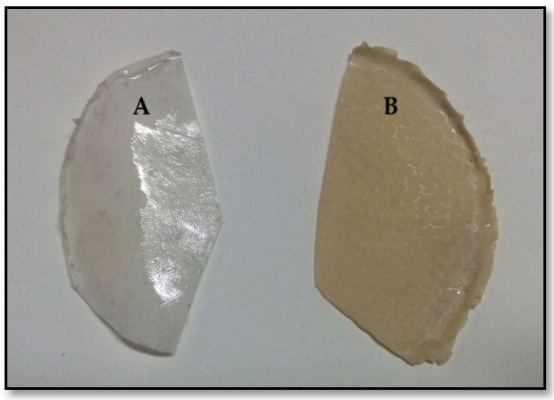

Figure 3.13. *PS-TiO_2 composite before UV irradiation (A) and after UV irradiation of 1000 h (B)*

A slight yellowing and loss of transparency was observed in UV exposed PS and PS-composite sheets. UV exposure of the specimens also resulted in increased

brittleness. Increased surface roughness and accumulation of yellow powders of depleted polymer layers could also be observed over the surface. These physically observed facts suggested that a change in optical and mechanical properties of PS as well as PS composites had occurred as a consequence of UV irradiation (Figure 3.13).

3.5 Mechanism of Photodegradation of PS under UV radiation

Table 3.4 highlights the important observations and conclusions drawn from various monitoring techniques of PS, PS-TiO_2 and PS-ZnO photodegradation explained above based on which the mechanism of photodegradation was proposed. In general, we could conclude that photo-oxidation mechanism has taken place as revealed by FTIR spectra.

Table 3.4. *Observations and conclusions made from GPC, FTIR spectroscopy, UV-DRS, electrical studies, weight loss measurements and SEM.*

Observations (with the increase in UV exposure time)	Conclusions
GPC	
• Decrease in $\bar{M}_w$ and $\bar{M}_n$ • Increase in no: of chain scission per macro molecule (S) • Increase in scission events per gram (N_t) • Decrease in mechanical properties of PS (Tensile & Flexural strengths)	• -C-C- or -C-H bond of the polymer chain has ruptured upon UV exposure • Scission of polymer chains was random
Electrical Studies	
• Dielectric strength (BDV) has decreased • Dielectric constant has increased	• Formation of charge centers • Decrease in the capacitance property
FTIR	
• Increase in the intensity of peaks corresponding to >C=O, -OH, -OOH, >C=C<, conjugated >C=C< etc • No change in the intensity of peaks corresponding to phenolic stretch or bend.	• Formation of new >C=C< linkages • Formation of new >C=O groups • Formation of new –OH, -OOH etc. groups • Formation of new >C=C-C=C-C=C< (conjugation) • Phenolic ring remains intact
UV-DRS	
• Decrease in characteristic absorption peaks of PS.	• Loss of characteristic absorption of PS due to photodegradation.

• Peaks have shifted towards higher wavelength.	• Red shift (Which could also be observed as slight yellowing of PS after irradiation)
Bandgap energy (E_g) calculations	
• Reduces to lower energy	• The ability of polymer specimens to absorb UV radiation has decreased.
Thermal studies (TGA)	
• Decrease in decomposition temperature	• Thermal stability has decreased due to chain scission within PS
Weight loss measurements	
• Weight loss was observed	• Loss of volatile species/gases formed as a consequence of photodegradation of PS
SEM	• Change in surface morphology of PS

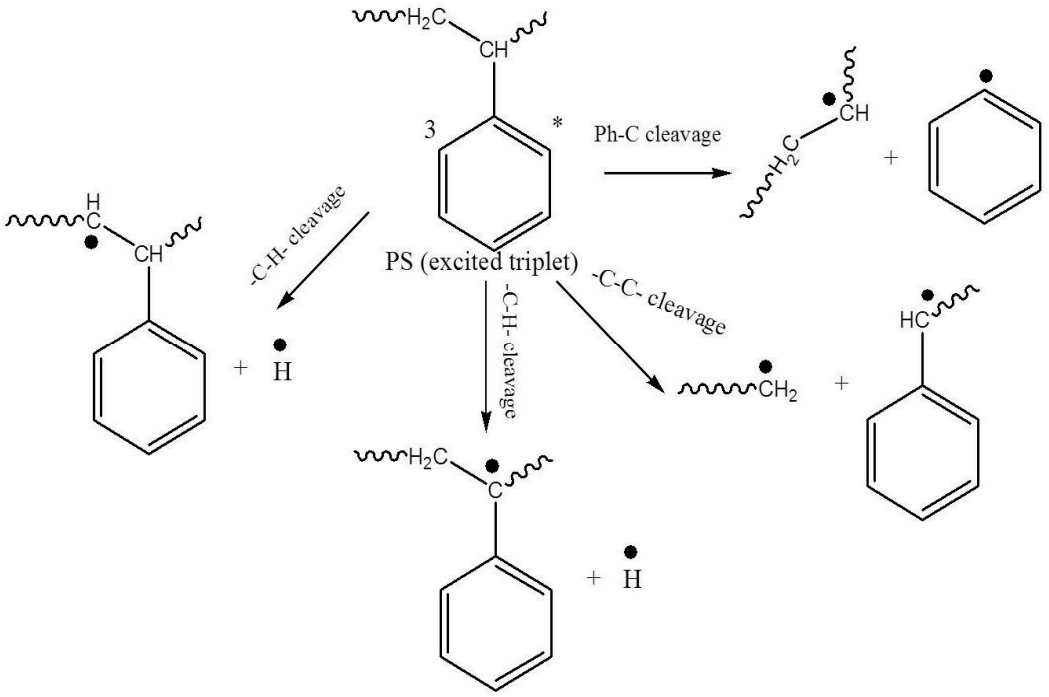

Figure 3.14.1. *Possible -C-C- and/or -C-H- bond scissions at various sites of PS.*

Mechanism of photodegradation of PS followed random pathways due to the multiple possibility of bond breakage, bond recombination, addition or elimination of various atoms. Based on all the above observations summarised in Table 3.4 the following mechanism could be considered.

Photodegradation starts with the phenolic rings of PS absorbing UV radiation and getting excited into singlet states and then undergoing an inter system crossing (ISC) into excited triplet states. Various photochemical reactions originate from excited

triplet state of benzene rings in PS. As evident from GPC data, -C-C- and/or -C-H- bond scissions at various sites could be initiated (Figure 3.14.1). FTIR spectra shows the evidence of formation of alkenic >C=C< double bonds and conjugated double bonds. This could be possible when cleavage of -C-H bonds belonging to adjacent carbons occur as represented in Figure 3.14.2.

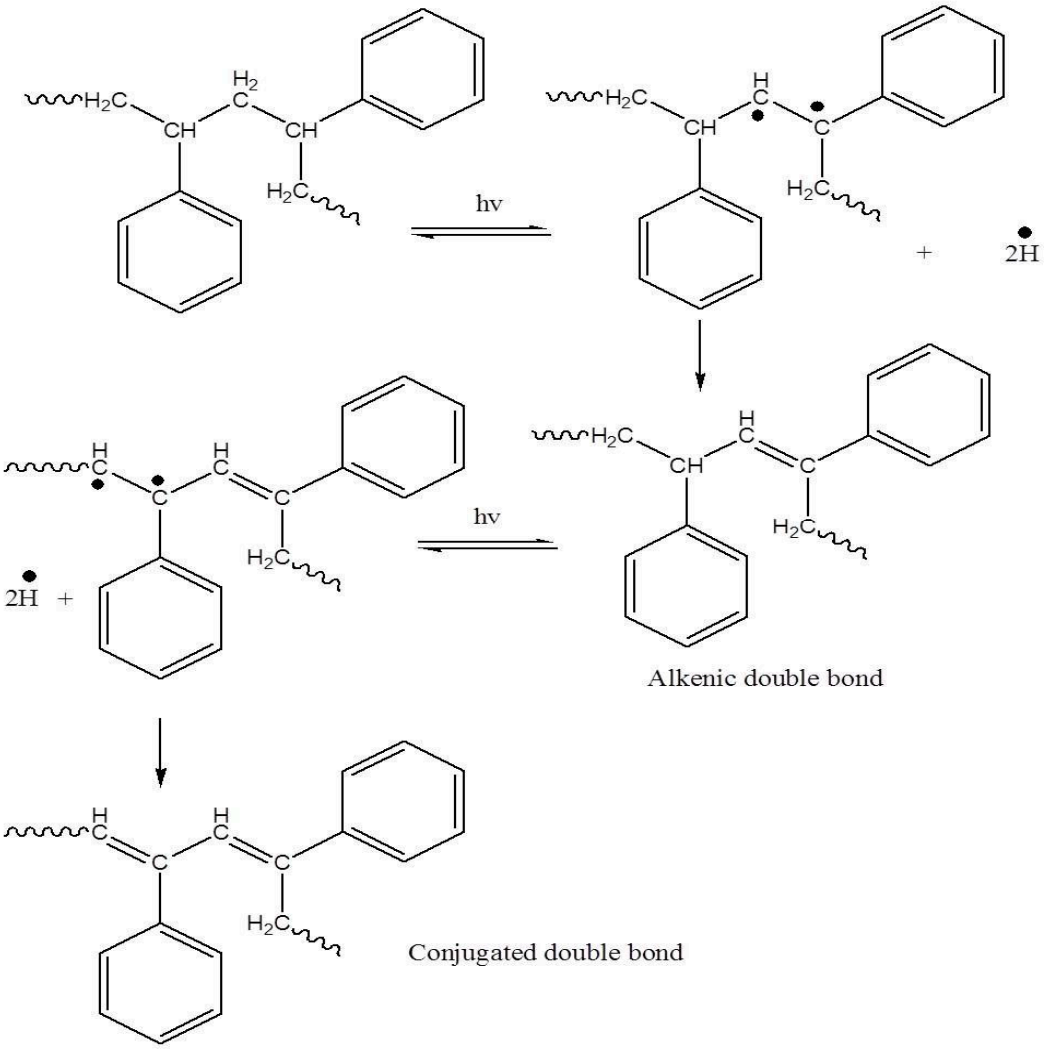

Figure 3.14.2. *Formation of C=C double bond and conjugated double bonds.*

Formation of >C=O, -OOH, -OH etc., groups were also evident from FTIR spectra. This could only be possible due to the adsorption of H_2O and O_2 molecules on the surface of PS. H_2O and O_2 could also be trapped on PS as impurities during the time of its manufacture. These molecules form reactive radicals or ions when interacted with incoming UV radiations. The radicals or ions could further interact

with PS chain forming macromolecular radicals or ions. The possible mechanism is as illustrated in Figure 3.14.3.

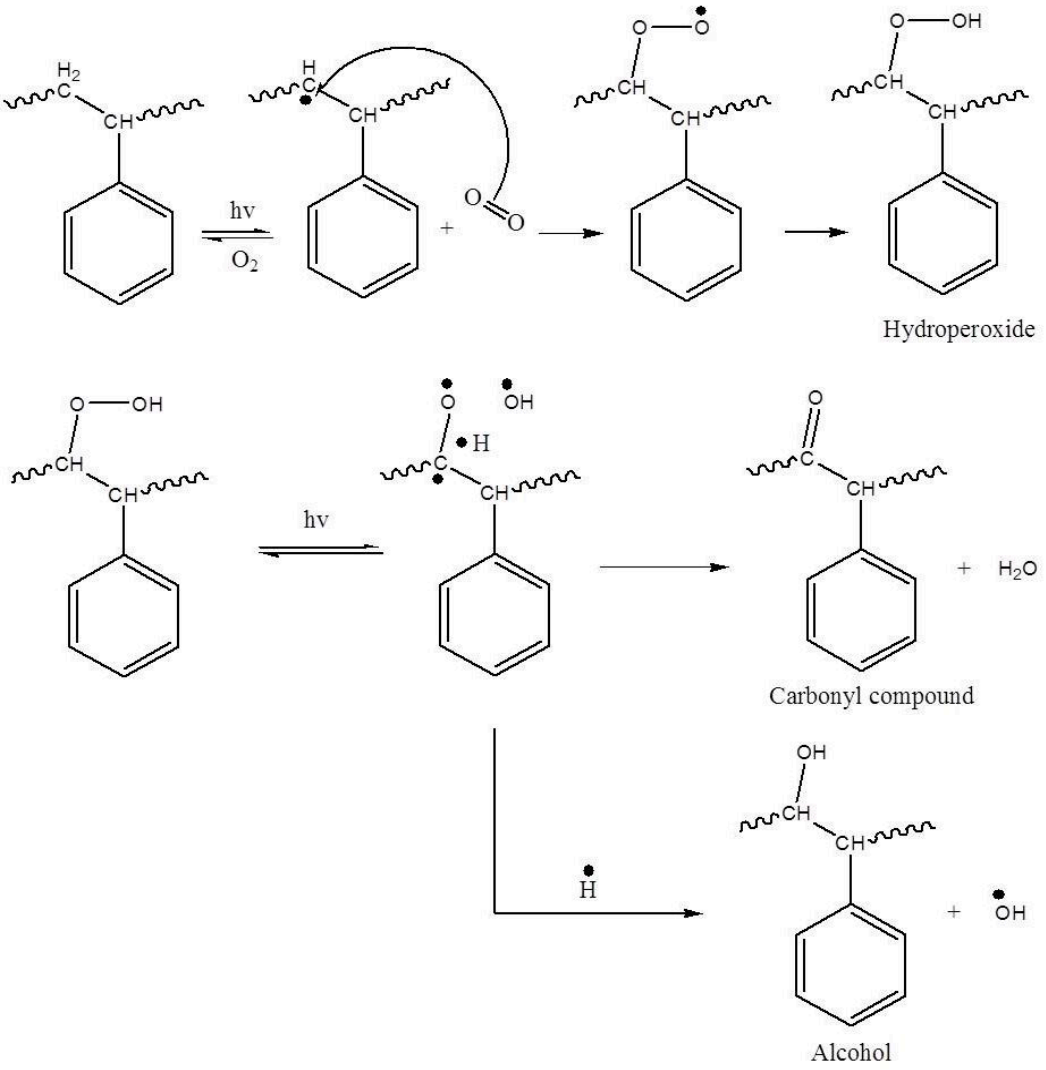

Figure 3.14.3. *Formation of –OOH, >C=O and –OH.*

Results of various analyses discussed above supported the fact that the rate of photodegradation of PS increased in the presence of nano TiO_2 as well as nano ZnO photocatalyst. It was also found that increase in the percentage of catalyst loaded to PS matrix showed no observable shift (red or blue shift) in the characteristic IR bands of PS. This observation made it clear that there existed no chemical bond between PS and TiO_2. The interaction between PS and TiO_2 was just physical. The mechanism of photodegradation of PS-TiO_2 and PS-ZnO composite occurs not only by PS absorbing UV radiations to get excited but also by nano TiO_2 and nano ZnO particles absorbing UV radiations creating electron-hole pair[49]. Electrons get excited from valence band

to conduction band leaving behind holes in valence band. Photocatalysis is possible only when the newly created electron-hole pair interacts with external atoms or molecules before recombining. Adsorbed O_2 molecules over the surface of ZnO or TiO_2 interact with the excited electrons in conduction band to form ions such as O^-, $O_2^{\bullet-}$ etc. H_2O or OH^- ions adsorbed on the surface of ZnO and TiO_2 results in the formation of H^+,$OH^\bullet$, OH^- etc species[50]. These newly created ions and radicals further interacts with PS chain forming hydroxides, hydroperoxides, carbonyl compounds etc. and the degradation process get propagated as illustrated through figure 3.14.1, 3.14.2 and 3.14.3.

3.6. Conclusion

Nano TiO_2 and ZnO particles were successfully synthesised and characterized. Sonication assisted sol-gel technique resulted in nano TiO_2 particles of spherical morphology. ZnO synthesised through sonication assisted precipitation results in nano ZnO particles resembling spheres with irregular edges. ZnO synthesis via hydrothermal method (controlled hydrolysis) resulted in spherical nano ZnO particles while that synthesised through hydrothermal method (uncontrolled hydrolysis) resulted in hexagonal ZnO rods of length reaching up to micro scale. Crystal growth occurred due to excess water resulted in larger size of these ZnO rods. XRD patterns of TiO_2 confirmed that anatase phase predominated over rutile phase. The synthesised nano TiO_2 and nano ZnO particles were successfully loaded into PS matrix whose photodegradation was studied in comparison with that of pristine PS. Photodegradation had taken place in solid phase PS sheets when subjected to UV irradiation (253 nm) under normal condition. Photodegradation of PS was proportional to UV irradiation time. The rate of photodegradation was higher in PS-TiO_2 and PS-ZnO composites and the rate of degradation increased with the increase in the percentage of photocatalysts loaded into PS matrix. The degradation of PS and PS-TiO_2 composite had taken place through photo-oxidative mechanism as evident from the increase in vibrational peaks corresponding to >C=O, -OH, -OOH, >C=C< and conjugated double bonds observed in FTIR spectroscopy upon UV irradiation. Through UV-DRS, changes in regular absorption bands in the UV region were also observed for PS, PS-TiO_2 and PS-ZnO composites upon irradiation. Weight loss of PS-composites was more compared to pristine PS films upon increase in UV

irradiation time. Tensile and flexural properties of PS as well as PS- composites decreased with the increase in the time of irradiation. Dielectric strength of the specimens increased with UV exposure time. The decrease in dielectric breakdown values measured in AC at a frequency of 50 Hz suggested the formation of charged centers upon UV irradiation. These results highlighted the fact that depletion in mechanical, electrical and chemical properties has taken place as a result of UV irradiation of PS, PS-TiO_2 and PS-ZnO composites. Better photocatalytic efficiency for the degradation of PS was exhibited by nano TiO_2 in comparison with nano ZnO particles.

References

1. Yousif, E. & Haddad, R. Photodegradation and photostabilization of polymers, especially polystyrene: review. *Springerplus* **2**, 398 (2013).
2. Ali, G. Q. *et al.* Photostability and Performance of Polystyrene Films Containing 1,2,4-Triazole-3-thiol Ring System Schiff Bases. *Molecules* **21**, (2016).
3. Grassie, N. & Weir, N. A. The photooxidation of polymers. IV. A note on the coloration of polystyrene. *J. Appl. Polym. Sci.* **9**, 999–1003 (1965).
4. Rabek, J. & Ranby, B. Studied on the photooxidation mechanism of polymers, photolysis and photooxidation of polystyrene. *J. Polym. Sci.* **12**, (1974).
5. Lucki, J. & Rånby, B. Photo-oxidation of polystyrene—Part I. Formation of hydroperoxide groups in photo-oxidised polystyrene and 2-phenyl butane. *Polym. Degrad. Stab.* **1**, 1–16 (1979).
6. Al Safi, S. A., Al Mouamin, T. M., Al Sieadi, W. N. & Al Ani, K. E. Irradiation Effect on Photodegradation of Pure and Plasticized Poly (4-Methylstyrene) in Solid Films. *Mater. Sci. Appl.* **5**, 300 (2014).
7. Jane, M., Tryon, M. & Achhammer, B. G. Study of degradation of polystyrene, using ultraviolet spectrophotometry. *J. Res. Natl. Bur. Stand. (1934).* **51**, (1953).
8. Timóteo, G. A. V, Fechine, G. J. M. & Rabello, M. S. Stress Cracking and Photodegradation: The Combination of Two Major Causes of HIPS Failure. *Macromol. Symp.* **258**, 162–169 (2007).
9. Ani, K. E. Al & Ramadhan, A. E. Photodegradation kinetics of poly(para-substituted styrene) in solution. *Polym. Degrad. Stab.* **93**, 1590–1596 (2008).
10. Rincón G., A. Photodegradation of chain halogenated polystyrene: Poly (c-chloro and c-bromostyrene)s. *Polym. Bull.* **38**, 191–196 (1997).
11. Gewert, B., Plassmann, M., Sandblom, O. & MacLeod, M. Identification of Chain Scission Products Released to Water by Plastic Exposed to Ultraviolet Light. *Environ. Sci. Technol. Lett.* **5**, 272–276 (2018).
12. Lei, Y., Lei, H. & Huo, J. Innovative controllable photocatalytic degradation of polystyrene with hindered amine modified aromatic polyamide dendrimer/ polystyrene-grafted-TiO2 photocatalyst under solar light irradiation. *Polym. Degrad. Stab.* **118**, 1–9 (2015).
13. Retamoso, C. *et al.* Effect of particle size on the photocatalytic activity of modified rutile sand (TiO2) for the discoloration of methylene blue in water. *J. Photochem. Photobiol. A Chem.* **378**, 136–141 (2019).
14. Dodd, A. C., McKinley, A. J., Saunders, M. & Tsuzuki, T. Effect of Particle Size on the Photocatalytic Activity of Nanoparticulate Zinc Oxide. *J. Nanoparticle Res.* **8**, 43 (2006).
15. Adhikari, S. & Lachgar, A. Effect of particle size on the photocatalytic activity of

BiNbO4 under visible light irradiation. in *Journal of Physics: Conference Series* vol. 758 (2016).
16. Khan, M. M., Adil, S. F. & Al-Mayouf, A. Metal oxides as photocatalysts. *J. Saudi Chem. Soc.* **19**, 462–464 (2015).
17. Riente, P. & Noël, T. Application of metal oxide semiconductors in light-driven organic transformations. *Catal. Sci. Technol.* **9**, 5186–5232 (2019).
18. Kiriakidis, G. & Binas, V. Metal oxide semiconductors as visible light photocatalysts. *J. Korean Phys. Soc.* **65**, 297–302 (2014).
19. Pelizzetti, E. & Minero, C. Metal Oxides as Photocatalysts for Environmental Detoxification. *Comments Inorg. Chem.* **15**, 297–337 (1994).
20. Kamat, P. V & Meisel, D. Nanoscience opportunities in environmental remediation. *Comptes Rendus Chime* **6**, 999–1007 (2003).
21. Kumar, S. G. & Rao, K. S. R. K. Comparison of modification strategies towards enhanced charge carrier separation and photocatalytic degradation activity of metal oxide semiconductors (TiO2, WO3 and ZnO). *Appl. Surf. Sci.* **31517**–**3**, S0169-4332 (2016).
22. Chen, D. & Ray, A. K. Removal of toxic metal ions from wastewater by semiconductor photocatalysis. *Chem. Eng. Sci.* **56**, 1561–1570 (2001).
23. He, J.-A., Mosurkal, R., Samuelson, L. A., Li, L. & Kumar, J. Dye-sensitized Solar Cell Fabricated by Electrostatic Layer-by-Layer Assembly of Amphoteric TiO2 Nanoparticles. *Langmuir* **19**, 2169–2174 (2003).
24. Chen, X. & Mao, S. S. Titanium Dioxide Nanomaterials: Synthesis, Properties, Modifications, and Applications. *Chem. Rev.* **107**, 2891–2959 (2007).
25. Vijayalakshmi, R. & Rajendran, V. Synthesis and characterization of nano-TiO 2 via different methods. **4**, 1183–1190 (2012).
26. Thomas, R. T., Nair, V. & Sandhyarani, N. TiO2 nanoparticle assisted solid phase photocatalytic degradation of polythene film: A mechanistic investigation. *Colloids Surfaces A Physicochem. Eng. Asp.* **422**, 1–9 (2013).
27. Kavitha, T; Rajendran, A. D. A. Synthesis and Characterization of Nanosized TiO2 Powder Derived From a Sol-Gel Process an Acidic Condition. *Int. J. Eng. Sci. Emerg. Technol.* **4**, 90–95 (2013).
28. Kavitha, T., Rajendran, A. & Durairajan, A. Synthesis, characterization of TiO2 nano powder and water based nanofluids using two step method. *Eur. J. Appl. Eng. Sci. Res.* **1**, 235–240 (2012).
29. Baruwati, B., Kumar, D. K. & Manorama, S. V. Hydrothermal synthesis of highly crystalline ZnO nanoparticles : A competitive sensor for LPG and EtOH. *Sensors Actuators B* **119**, 676–682 (2006).
30. Arami, H., Mazloumi, M., Khalifehzadeh, R. & Sadrnezhaad, S. K. Sonochemical preparation of TiO2 nanoparticles. *Mater. Lett.* **61**, 4559–4561 (2007).
31. Thamaphat, K., Limsuwan, P., Ngotawornchai, B. & others. Phase characterization of TiO2 powder by XRD and TEM. *Kasetsart J.(Nat. Sci.)* **42**, 357–361 (2008).
32. Hassanjani-Roshan, A., Kazemzadeh, S. M., Vaezi, M. R. & Shokuhfar, A. Effect of sonication power on the sonochemical synthesis of titania nanoparticles. *J. Ceram. Process. Res.* **12**, 299–303 (2011).
33. Byrne, C., Fagan, R., Hinder, S., McCormack, D. E. & Pillai, S. C. New approach of modifying the anatase to rutile transition temperature in TiO2 photocatalysts. *RSC Adv.* **6**, 95232–95238 (2016).
34. Lee, H. Y. & Kale, G. M. Hydrothermal Synthesis and Characterization of Nano-TiO2. *Int. J. Appl. Ceram. Technol.* **665**, 657–665 (2008).
35. Tian, J. *et al.* Photocatalyst of TiO2/ZnO nano composite film: Preparation, characterization, and photodegradation activity of methyl orange. *Surf. Coatings Technol.* **204**, 205–214 (2009).
36. López, R. & Gómez, R. Band-gap energy estimation from diffuse reflectance measurements on sol-gel and commercial TiO2: a comparative study. *J. Sol-Gel Sci. Technol.* **61**, 1–7 (2012).

37. Reddy, K. M., Manorama, S. V & Reddy, A. R. Bandgap studies on anatase titanium dioxide nanoparticles. *Mater. Chem. Phys.* **78**, 239–245 (2003).
38. Chandran, A., Francis, N., Jose, T. & George, K. Synthesis, structural characterization and optical bandgap determination of ZnS nanoparticles. *SB Acad. Rev.* **17**, 17–21 (2010).
39. Jaleh, B. *et al.* UV-degradation effect on optical and surface properties of polystyrene-TiO2 nanocomposite film. *J. Iran. Chem. Soc.* **8**, S161--S168 (2011).
40. Abdelghany, A. M., Abdelrazek, E. M., Badr, S. I. & Morsi, M. A. Effect of gamma-irradiation on (PEO/PVP)/Au nanocomposite: Materials for electrochemical and optical applications. *Mater. Des.* **97**, 532–543 (2016).
41. Sangawar, V. & Golchha, M. Evolution of the optical properties of Polystyrene thin films filled with Zinc Oxide nanoparticles. *Int J Sci Eng Res* **4**, 2700–2705 (2013).
42. Alwan, T. J. Refractive index dispersion and optical properties of dye doped Polystyrene films. *Malaysian Polym. J.* **5**, 204–213 (2010).
43. Sirohi, S. & Sharma, T. P. Bandgaps of cadmium telluride sintered film. *Opt. Mater. (Amst).* **13**, 267–269 (1999).
44. Wang, D., Huang, M., Zha, J., Zhao, J. & Dang, Z. Dielectric Properties of Polystyrene Based Composites Filled with Core-Shell BaTiO 3 / Polystyrene Hybrid Nanoparticles. *IEEE Trans. Dielectr. Electr. Insul.* **21**, 1438–1445 (2014).
45. Rao, Y., Qu, J., Marinis, T. & Wong, C. P. A precise numerical prediction of effective dielectric constant for polymer-ceramic composite based on effective-medium theory. *IEEE Trans. Components Packag. Technol.* **23**, 680–683 (2000).
46. Grove, T. T., Masters, M. F. & Miers, R. E. Determining dielectric constants using a parallel plate capacitor. *Am. J. Phys.* **73**, 52–56 (2005).
47. Hwang, D., Shul, Y. & Chu, Y. Photodegradation behavior of the polycarbonate/TiO2 composite films under the UV irradiation in ambient air condition. *Polym. Compos.* **36**, 1462–1468 (2014).
48. Cho, S. & Choi, W. Solid-phase photocatalytic degradation of PVC–TiO2 polymer composites. *J. Photochem. Photobiol. A Chem.* **143**, 221–228 (2001).
49. Shang, J., Chai, M. & Zhu, Y. Solid-phase photocatalytic degradation of polystyrene plastic with TiO2 as photocatalyst. *J. Solid State Chem.* **174**, 104–110 (2003).
50. Nagaveni, K., Hegde, M. S., Ravishankar, N. & Subbanna, G. N. Synthesis and Structure of Nanocrystalline TiO 2 with Lower Band Gap Showing High Photocatalytic Activity. *Langmuir* **9**, 2900–2907 (2004).